We also examined the relative SMC3, RAD21 and SMC1A levels in human oocytes (Figs. 1 and 3A–C). In contrast to the meiosis-specific cohesins, the signal intensities of these proteins did not significantly change with age, although a slight decrease in the SMC1A level was evident in oocytes of older women (Fig. 3D–F).

Cohesins in the dictyate oocytes of the mouse

To evaluate whether our above findings are unique to humans in which a long life span leads to years of dictyate arrest, we performed similar immunofluorescence experiments in the mouse. Two-month-old and 10-month-old wild-type B6 mice, which have just become sexually matured and have reached the late reproductive age, respectively, were examined (Fig. 4). In each age group, samples were derived from 3 mice. The signal intensity of REC8 in the older mice was significantly lower than that of younger mice (Fig. 5A, C, D) as demonstrated in our human analyses (Fig. 2). Likewise, the signal intensity of SMC1B in older mice was also low relative to that of younger mice (Fig. 5B, C, D). Thus, meiosis-specific cohesins in mouse oocytes decrease in an age-related manner as with humans.

We found from our immunofluorescence analyses that the signal intensity of SMC3 in older mice was not significantly different from that of younger mice. This result is similar to that found in humans, although the signal intensities of oocytes to somatic cells in mice were found to be slightly lower than those in humans (Fig. 6A, D, E). In contrast, the signal intensity of RAD21 in older mice showed a slight increase compared with younger mice (Fig. 6B, D, E). Interestingly, and in contrast to humans, the immunofluorescent signal intensity of SMC1A in the nuclei of mouse oocytes was barely detectable relative to that in somatic cells (Figs. 1D and 4C). Although the mean signal intensity of SMC1A in each older mouse was almost similar to that in each younger mouse (Fig. 6C, D), the mean signal intensity in each oocyte was increased slightly in older mice, as was observed for RAD21 (Fig. 6E).

Discussion

Age-related decrease in meiosis-specific cohesin subunits

In our present study, we demonstrate an age-related decrease of meiosis- specific cohesin subunits, REC8 and SMC1B, in dictyate oocytes both in humans and mice. In contrast, the signal levels of the cohesin subunits common to mitotic cells, SMC3, RAD21 and SMC1A, did not change. To our knowledge, this is the first report to demonstrate an age-related decrease in the cohesin concentrations in human oocytes at the protein level. Although it has been reported that cohesin staining in MI and MII oocytes from women of different ages (age range: 18–34) indicated no decrease in the older women [18], this may be possibly attributed to the samples derived from relatively young women compared to our present study.

It has been long accepted that age-related increases in oocyte aneuploidy do not occur in mice. Long dictyate arrest in humans due to a long life span is likely to underlie this difference. However, age-related aneuploidy has been detected in certain mouse strains such as C57BL/6 [19,20]. Indeed, age-related decreases in REC8 have been reported previously in the C57BL-related strains [11,12]. It is therefore currently believed that this phenomenon is strain-dependent. These findings are consistent with the linkage between the age–related increase of aneuploidy and decrease in cohesin levels seen also in humans.

The mechanism of reduction in cohesin levels on the chromatin in dictyate oocytes remains to be clarified. Oxidative damage or spontaneous hydrolysis of peptide bonds that are generally involved in protein aging are one possible cause of this degradation [13]. It has also been suggested that leaky separase activity may cause a loss of cohesins [13,21]. Although separase intrinsically cleaves the cohesin ring at anaphase onset [22]. the expression

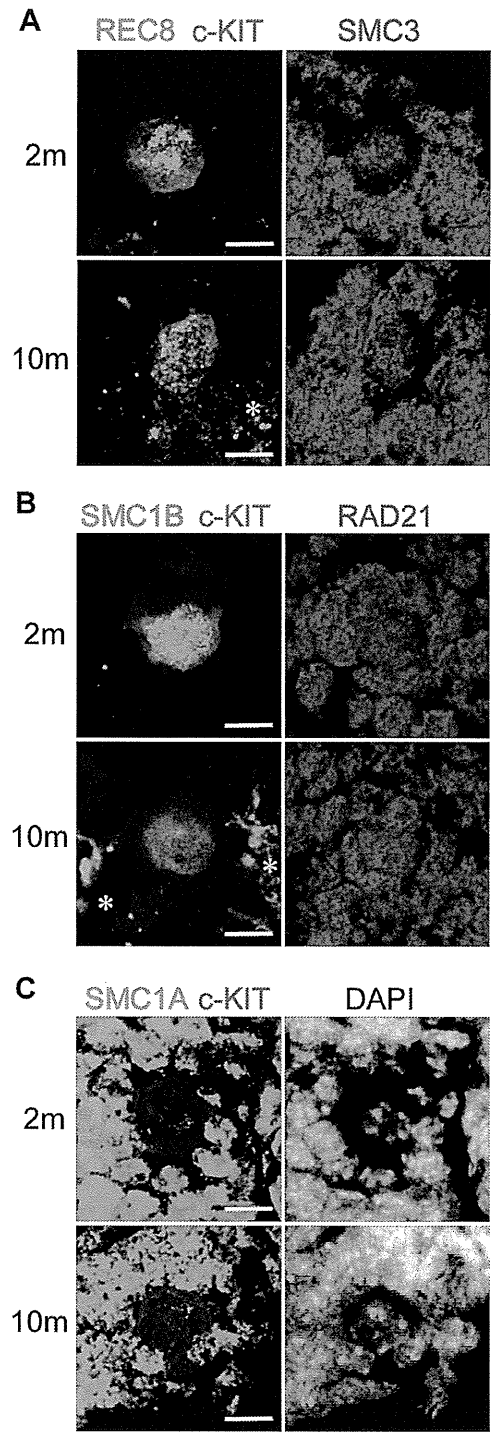

Figure 4. Immunofluorescent staining of mouse oocytes in ovarian sections from 2- and 10-month-old female mice. (A) Slides were co-immunostained with REC8 (green) and SMC3 (red). (B) Slides were co-immunostained with SMC1B (green) and RAD21 (red). (C) SMC1A (green) signals with DAPI nuclear counterstaining. Asterisks indicate autofluorescence. Bar, 10 μm.
doi:10.1371/journal.pone.0096710.g004

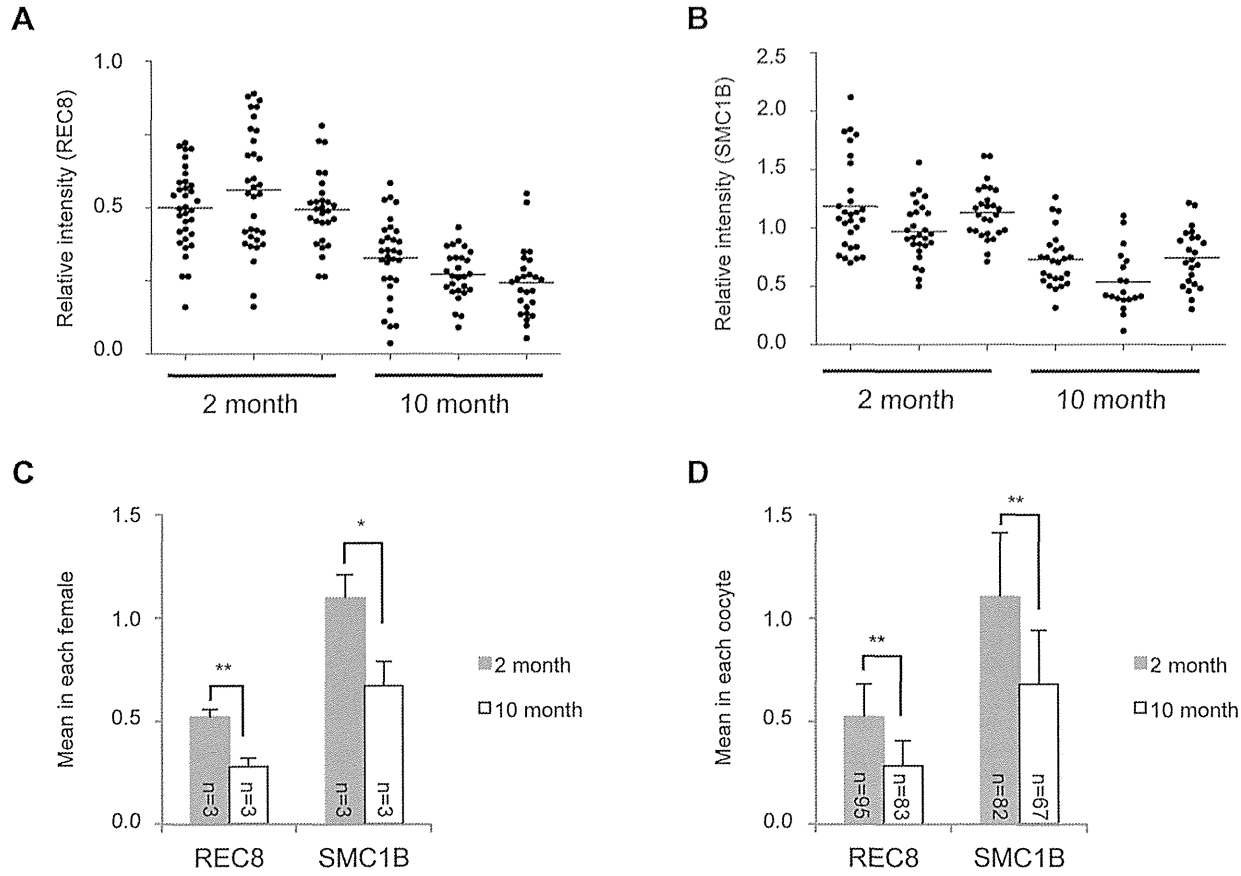

Figure 5. Quantitative results for meiosis-specific cohesin levels in 2- and 10-month-old mouse oocytes. (A, B) Relative signal intensity of REC8 or SMC1B. Intensities were determined as indicated in Figure S2. Three mice were used at each age. Horizontal bars are the mean cohesin levels within each female. (C) Cohesin signal intensity means in each female (mean ± SD). (D) Cohesin signal intensity means in each oocyte (mean ± SD). *$P<0.05$, **$P<0.01$, Student's t-test.
doi:10.1371/journal.pone.0096710.g005

level of this enzyme was previously found to be up-regulated in metaphase II oocytes in older women compared with younger [23].

The expression patterns of cohesin mRNAs in human oocytes determined by microarray analyses were reported previously [23,24]. Whilst SMC3, RAD21 and SMC1A mRNAs are substantially expressed in oocytes, REC8 and SMC1B transcripts were only weakly detectable in these experiments. Thus, once meiosis-specific cohesin subunits undergo degradation, they would not undergo turnover in human or mouse, which facilitates the age-related decrease in the meiotic cohesin levels [9,10].

Coordination of meiotic and mitotic cohesins

Whilst the meiotic cohesins in mouse oocytes of a certain strain decrease within a few months, the cohesins are retained for decades in humans. It is tempting to imagine that special safeguarding mechanism had to be evolved in the long-living humans, and those mechanisms are absent in mice. We speculate that mitotic and meiotic cohesins may coordinately contribute maintaining the cohesion levels for long periods in humans. In our current study, we show that the SMC1A level was comparable between oocytes and somatic cells in humans, but only marginally detectable in mice. Based on the amino acid sequence of its epitope, the anti-SMC1A antibody used for detection of human SMC1A will not cross react with human SMC1B which is present in oocytes. It is suggested that both SMC1A-RAD21 and SMC1B-REC8 cohesins are present in human oocytes, and that SMC1A-RAD21 undergoes turnover even during dictyate arrest. This might partly contribute to maintaining the cohesin levels for a prolonged period in humans. In addition, the signal intensities of RAD21 and SMC1A were found to be slightly increased in aged mice in our present experiments. We suggest that this is supportive evidence for the upregulation of the mitotic cohesins in mouse oocytes to compensate for the loss of meiosis-specific cohesins. However, it has been shown that the SMC1A level is too marginal to compensate for the reduction in SMC1B in the mouse [25]. Nonetheless, no increase in SMC1A or RAD21 has been observed in human in accordance with the decrease in their meiotic counterparts, SMC1B and REC8. Even the baseline levels of SMC1A and RAD21 in human are still not sufficient to completely compensate for the loss of meiosis-specific cohesins. It is possible in this regard that the newly synthesized cohesins may be less able to hold sister chromatids together during meiosis since the cohesion establishment factors are not recruited without the DNA replication machinery [26,27].

Age-related decrease in cohesin and increase in aneuploidy

The frequency of trisomy in conceptuses is 2–3% in women aged in their twenties, but it rises exponentially in women in their mid-thirties to reach 35% in women aged over 40 [1]. However, the meiosis-specific cohesin levels in our current experiments

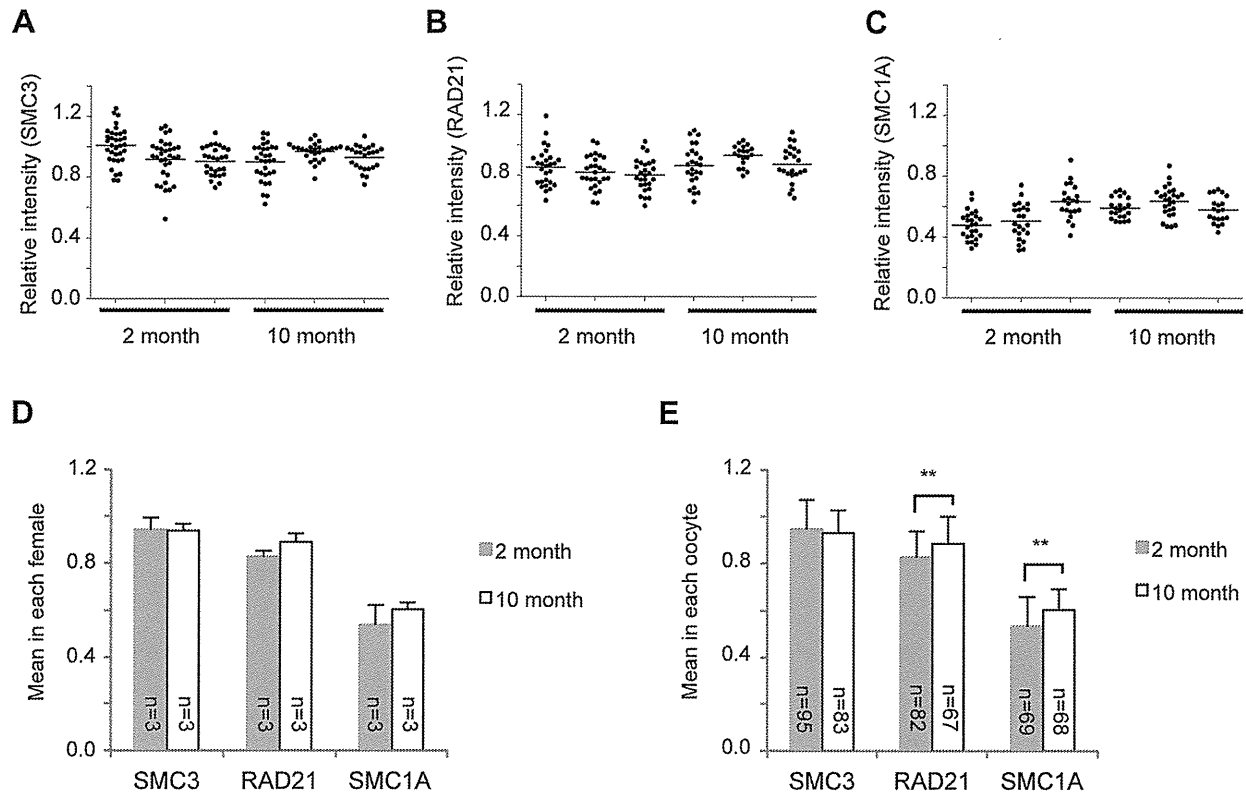

Figure 6. Quantitative results for mitotic cohesin levels in mouse oocytes. (A–C) Signal intensities for SMC3, RAD21 or SMC1A determined as described in Figure S2. (D) Cohesin signal intensity means in each female (mean ± SD). (E) Cohesin signal intensity means in each oocyte (mean ± SD). $^{**}P<0.01$, Student's *t*-test.
doi:10.1371/journal.pone.0096710.g006

showed a linear negative correlation with the age of the sample donors. As a cause of this disparity, one possibility is a threshold effect of the cohesin level with regard to segregation error susceptibility i.e. there may be a threshold level of cohesins that can hold sister chromatids together against physical force. We thus speculate that the meiotic chromosomes may undergo malsegregation until these levels reach this threshold.

An alternative possibility is that the cohesins, in regulating gene expression, are involved in the exponential increase in aneuploidy. Cohesin depletion may cause a substantial effect on gene expression through defects in transcriptional regulatory functions [8,28,29]. Indeed, the expression of various genes in mature oocytes has been shown to change with age [23,30,31]. Thus, the chromosomes with impaired cohesions would be more susceptible to segregation error possibly because of spindle checkpoint defects caused by altered gene expression [23,32].

In accordance with the results of our present study, the age-related increase of interkinetochore distance between sister chromatids has been observed in the metaphase II oocytes of humans, suggesting a deterioration of chromosome cohesion with advancing age [33]. Without replenishment of meiosis-specific cohesins, cohesion between sister chromatids gradually deteriorates over time. This causes premature resolution of the chiasma between homologs or the premature separation of sister chromatids during the dictyate stage. Since these pre-separated chromosomes are distributed into daughter cells randomly, they are prone to malsegregation leading to gametes with aneuploidy. In our present study, besides the age-effect, we observed a variation among individuals in the rate of cohesin decrease. This might be due to the differences in genetic background and/or lifestyle. In future studies, a determination of the genetic variation affecting cohesin robustness will help to predict the susceptibility of individuals. A further elucidation of the mechanism underlying the decrease or maintenance of meiotic cohesins will contribute to the development of novel strategies to prevent age-related aneuploidy.

Supporting Information

Figure S1 Specificity of the antibodies. (A) Western blot analysis using affinity-purified antibodies. Testes lysates from human or mouse were loaded on the same gel. After electrophoresis and blotting, blots were stained with Ponceau S, and the each lane was cut into strips. SMC1B and REC8 were detected as 145-kDa and 75- to 82-kDa bands, respectively. Asterisks and dots indicate nonspecific bands reacted with the secondary antibodies. (B) Negative control of cohesin-immunostaining using IgGs and the secondary antibodies. (C) Negative control of cohesin-immunostaining using preimmune sera. (D) Negative control of cohesin-immunostaining using antibodies absorbed by preincubation with the peptide immunogens.
(PDF)

Figure S2 Representative immunofluorescent staining pattern of human oocytes. Green and blue signal intensities within the circled areas, indicating the oocyte nucleus, were respectively determined, as well as 5 randomly chosen somatic nuclei in the vicinity of the oocyte. The signal intensity of REC8 (green) was defined as: (area density of green signal in oocyte nucleus - mean area density of green signal in 5 somatic nuclei)/ mean area density of blue staining in 5 somatic nuclei. Because the

green signals detected in somatic nuclei are background, these were subtracted from the signals in the oocytes. The signals in the oocytes were adjusted using the blue signal corresponding to the RAD21 cohesin subunit that is constitutively expressed in somatic cells. The signal intensity for RAD21 was defined as: area density of blue signal in the oocyte nucleus/mean area density of blue signal in 5 somatic nuclei.
(PDF)

Figure S3 Quantitative results for REC8 in human oocytes adjusted for the histone signals of somatic nuclei. (A) Immunofluorescent staining of human oocytes in ovarian sections from 19- and 49- year-old women. REC8 (green) proteins co-immunostained with histone (red) using anti-histone antibody (1:400; H11-4; Millipore). C-KIT (blue) was used as a marker of oocytes. Asterisks indicate autofluorescence in the cytoplasmic region of the oocytes. Bar, 10 μm. (B) Relative signal intensity of REC8. Intensities were determined as described in Figure S2, more specifically, histone signal in somatic nuclei was used to adjust the REC8 signal intensity. Specimens were obtained from 4 women (age range: 19–49 years). (C) Regression analysis of the REC8 signal intensity means shown in (B) (mean ± SD). Line indicates the regression line. The coefficient of determination is in parenthesis. (D) Comparisons of the signal intensity means between grouped samples. Women were grouped as indicated in Figure 2. The REC8 signal intensity means in single oocytes were compared between groups (mean ± SD). $^{**}P<0.01$, Student's *t*-test.
(PDF)

Table S1 Antibodies used in this study.
(PDF)

Acknowledgments

We thank S. Ikeda and S. Hamada-Tsutsumi for technical assistance.

Author Contributions

Conceived and designed the experiments: MT RF HN HK HI TO TK HK. Performed the experiments: MT RF MI. Analyzed the data: MT RF HK MI HI TO TK HK. Wrote the paper: MT HN HK HI TO TK HK. Provided human tissues: HN TF.

References

1. Hassold T, Hunt P (2001) To err (meiotically) is human: the genesis of human aneuploidy. Nat Rev Genet 2: 280–291.
2. Hassold T, Hall H, Hunt P (2007) The origin of human aneuploidy: where we have been, where we are going. Hum Mol Genet 16: R203–208.
3. Yoon PW, Freeman SB, Sherman SL, Taft LF, Gu Y, et al. (1996) Advanced maternal age and the risk of Down syndrome characterized by the meiotic stage of chromosomal error: a population-based study. Am J Hum Genet 58: 628–633.
4. Grande M, Borrell A, Garcia-Posada R, Borobio V, Muñoz M, et al (2012). The effect of maternal age on chromosomal anomaly rate and spectrum in recurrent miscarriage. Hum Reprod 27: 3109–3117.
5. Nybo Andersen AM, Wohlfahrt J, Christens P, Olsen J, Melbye M (2000) Maternal age and fetal loss: population based register linkage study. BMJ 320: 1708–1712.
6. Revenkova E, Eijpe M, Heyting C, Hodges CA, Hunt PA, et al. (2004) Cohesin SMC1 beta is required for meiotic chromosome dynamics, sister chromatid cohesion and DNA recombination. Nat Cell Biol 6: 555–562.
7. Lee J, Okada K, Ogushi S, Miyano T, Miyake M, et al. (2006) Loss of Rec8 from chromosome arm and centromere region is required for homologous chromosome separation and sister chromatid separation, respectively, in mammalian meiosis. Cell Cycle 5: 1448–1455.
8. Wood AJ, Severson AF, Meyer BJ (2010) Condensin and cohesin complexity: the expanding repertoire of functions. Nat Rev Genet 11: 391–404.
9. Revenkova E, Herrmann K, Adelfalk C, Jessberger R (2010) Oocyte cohesin expression restricted to predictyate stages provides full fertility and prevents aneuploidy. Curr Biol 20: 1529–1533.
10. Tachibana-Konwalski K, Godwin J, van der Weyden L, Champion L, Kudo NR, et al. (2010) Rec8-containing cohesin maintains bivalents without turnover during the growing phase of mouse oocytes. Genes Dev 24: 2505–2516.
11. Chiang T, Duncan FE, Schindler K, Schultz RM, Lampson MA (2010) Evidence that weakened centromere cohesion is a leading cause of age-related aneuploidy in oocytes. Curr Biol 20: 1522–1528.
12. Lister LM, Kouznetsova A, Hyslop LA, Kalleas D, Pace SL, et al. (2010) Age-related meiotic segregation errors in mammalian oocytes are preceded by depletion of cohesin and Sgo2. Curr Biol 20: 1511–1521.
13. Jessberger R (2012) Age-related aneuploidy through cohesion exhaustion. EMBO Rep 13: 539–546.
14. Kurahashi H, Tsutsumi M, Nishiyama S, Kogo H, Inagaki H, et al. (2012) Molecular basis of maternal age-related increase in oocyte aneuploidy. Congenit Anom (Kyoto) 52: 8–15.
15. Kouznetsova A, Novak I, Jessberger R, Höög C (2005) SYCP2 and SYCP3 are required for cohesin core integrity at diplotene but not for centromere cohesion at the first meiotic division. J Cell Sci 118: 2271–2278.
16. Eijpe M, Heyting C, Gross B, Jessberger R (2000) Association of mammalian SMC1 and SMC3 proteins with meiotic chromosomes and synaptonemal complexes. J Cell Sci 113: 673–682.
17. Tsutsumi M, Kowa-Sugiyama H, Bolor H, Kogo H, Inagaki H, et al. (2012) Screening of genes involved in chromosome segregation during meiosis I: in vitro gene transfer to mouse fetal oocytes. J Hum Genet 57: 515–522.
18. Garcia-Cruz R, Brieño MA, Roig I, Grossmann M, Velilla E, et al. (2010) Dynamics of cohesin proteins REC8, STAG3, SMC1 beta and SMC3 are consistent with a role in sister chromatid cohesion during meiosis in human oocytes. Hum Reprod 25: 2316–2327.
19. Koehler KE, Schrump SE, Cherry JP, Hassold TJ, Hunt PA (2006) Near-human aneuploidy levels in female mice with homeologous chromosomes. Curr Biol 16: R579–580.
20. Selesniemi K, Lee HJ, Muhlhauser A, Tilly JL (2011) Prevention of maternal aging-associated oocyte aneuploidy and meiotic spindle defects in mice by dietary and genetic strategies. Proc Natl Acad Sci U S A 108: 12319–12324.
21. Chiang T, Schultz RM, Lampson MA (2011) Age-dependent susceptibility of chromosome cohesion to premature separase activation in mouse oocytes. Biol Reprod 85: 1279–1283.
22. Hauf S, Waizenegger IC, Peters JM (2001) Cohesin cleavage by separase required for anaphase and cytokinesis in human cells. Science 293: 1320–1323.
23. Grøndahl ML, Yding Andersen C, Bogstad J, Nielsen FC, Meinertz H, et al. (2010) Gene expression profiles of single human mature oocytes in relation to age. Hum Reprod 25: 957–968.
24. Markholt S, Grøndahl ML, Ernst EH, Andersen CY, Ernst E, et al. (2012) Global gene analysis of oocytes from early stages in human folliculogenesis shows high expression of novel genes in reproduction. Mol Hum Reprod 18: 96–110.
25. Bickel SE (2005) Aging (not so) gracefully. Nat Genet 37: 1303–1304.
26. Lengronne A, McIntyre J, Katou Y, Kanoh Y, Hopfner KP, et al. (2006) Establishment of sister chromatid cohesion at the S. cerevisiae replication fork. Mol Cell 23: 787–799.
27. Skibbens RV (2000) Holding your own: establishing sister chromatid cohesion. Genome Res 10: 1664–1671.
28. Nasmyth K, Haering CH (2009) Cohesin: its roles and mechanisms. Annu Rev Genet 43: 525–558.
29. Rudra S, Skibbens RV (2013) Cohesin codes - interpreting chromatin architecture and the many facets of cohesin function. J Cell Sci 126: 31–41.
30. Fragouli E, Bianchi V, Patrizio P, Obradors A, Huang Z, et al. (2010) Transcriptomic profiling of human oocytes: association of meiotic aneuploidy and altered oocyte gene expression. Mol Hum Reprod 16: 570–582.
31. Titus S, Li F, Stobezki R, Akula K, Unsal E, et al. (2013) Impairment of BRCA1-related DNA double-strand break repair leads to ovarian aging in mice and humans. Sci Transl Med 5: 172ra21.
32. Steuerwald N, Cohen J, Herrera RJ, Sandalinas M, Brenner CA (2001) Association between spindle assembly checkpoint expression and maternal age in human oocytes. Mol Hum Reprod 7: 49–55.
33. Duncan FE, Hornick JE, Lampson MA, Schultz RM, Shea LD, et al. (2012) Chromosome cohesion decreases in human eggs with advanced maternal age. Aging Cell 11: 1121–1124.

Journal of Human Genetics (2014), 1–4

www.nature.com/jhg

ORIGINAL ARTICLE

Signature of backward replication slippage at the copy number variation junction

Tamae Ohye[1], Hidehito Inagaki[1], Mamoru Ozaki[2], Toshiro Ikeda[3] and Hiroki Kurahashi[1]

Copy number abnormalities such as deletions and duplications give rise to a variety of medical problems and also manifest innocuous genomic variations. Aberrant DNA replication is suggested as the mechanism underlying *de novo* copy number abnormalities, but the precise details have remained unknown. In our present study, we analyzed the del(2)(q13q14.2) chromosomal junction site observed in a woman with a recurrent pregnancy loss. Microarray analyses allowed us to precisely demarcate a 2.8 Mb deletion in this case, which does not appear in the database of human genomic variations. This deletion includes only one brain-specific gene that could not be related to the reproduction failure of the patient. At the junction of the deletion, we found that 11–13-nucleotide sequence, originally located at the proximal breakpoint region, was repeated four times with a single-nucleotide microhomology at the joint between each repeat. The proximal region and the distal region was finally joined with six-nucleotide microhomology. The structure of the junction is consistent with backward replication slippage proposed previously. Our data lend support to the notion that a common DNA replication-mediated pathway generates copy number variation in the human genome.
Journal of Human Genetics advance online publication, 20 March 2014; doi:10.1038/jhg.2014.20

Keywords: backward replication slippage; copy number variation; deletion; DNA replication

INTRODUCTION

The mechanisms underlying gross chromosomal rearrangements (GCRs) including deletion/duplication, translocation and inversion are still largely unknown. Among the known GCRs, deletions and duplications give rise to a number of medical issues, such as congenital anomalies and intellectual disability that arise via copy number abnormalities of indispensable genes, and also manifest as innocuous polymorphic genomic variations.[1] GCR development is dependent on two intrinsic factors: double-strand breakage (DSB) and its illegitimate repair.[2] In general, DSBs will be correctly repaired by error-free pathways via homologous recombination. However, when DSBs arise within low-copy-repeat regions or segmental duplications, template anomalies may occur during DSB repair leading to chromosomal deletions or duplications. A subset of non-random deletions/duplications is caused by such non-allelic homologous recombination events between two homologous sequences, referred to as low-copy-repeat regions or segmental duplication.[3,4] Programmed DSBs by Spo11 endonuclease will cause meiotic recombination in meiosis I. These non-random deletions/duplications are mainly attributed to non-allelic homologous recombination in meiosis I.[5] On the other hand, most deletions or duplications take place in a random fashion. Deletions have been believed to arise from random DSBs followed by error-prone repair, such as non-homologous end joining, throughout the cell cycle particularly in G1 phase.[6]

Error-free homologous recombination has been believed to be a major pathway for DSB repair during S/G2 phase because sister chromatids are available.[6] In contrast, recent advances in genomic analyses using microarray or next generation sequencing technology have accumulated sequence information on breakpoints and junctions in random GCRs. The discovery of microhomology accompanied by complex structures at the junctions of copy number abnormalities raised the hypothesis for the involvement of aberrant DNA replication. Such a replication-based mechanism is referred to as fork stalling and template switching or as microhomology-mediated break-induced replication.[7,8] These mechanisms are on the basis of the collapse of the replication fork followed by a restart of DNA synthesis through the invasion by a free DNA end into another replication fork within close proximity.[8] In fact, nearly half of all deletions/duplications have been consistently revealed to carry microhomology at the junction.[9,10] However, the details of the underlying molecular pathway remain unknown in mammals.

In our present study, we characterized the genomic structure of the del(2)(q13q14.2) junction site, which was identified in a woman with

[1]Division of Molecular Genetics, Institute for Comprehensive Medical Science, Fujita Health University, Toyoake, Japan; [2]Division of Genomic Medicine, Department of Advanced Medicine, Medical Research Institute, Kanazawa Medical University, Ishikawa, Japan and [3]Department of Obstetrics and Gynecology, Faculty of Medicine, Kagoshima University, Kagoshima, Japan
Correspondence: Professor H Kurahashi, Division of Molecular Genetics, Institute for Comprehensive Medical Science, Fujita Health University, 1-98 Dengakugakubo, Kutsukake-cho, Toyoake, Aichi 470-1192, Japan.
E-mail: kura@fujita-hu.ac.jp
Received 2 December 2013; revised 7 February 2014; accepted 25 February 2014

a recurrent pregnancy loss. We provide supportive evidence for the involvement of aberrant DNA replication in the development of the underlying deletion.

MATERIALS AND METHODS

Subjects

A Japanese couple underwent cytogenetic examination due to two consecutive pregnancy losses. The karyotype of the male was 46,XY and that of the female was 46,XX,del(2)(q13q14.2). After informed consent was obtained, peripheral blood samples were obtained again from the woman for genomic analysis. No parental sample was obtained. This study was approved by the Ethical Review Board for Human Genome Studies at Fujita Health University (Accession number 86, approved on 12 March 2010).

Cytogenetic microarray

Cytogenetic microarray analysis was performed using Agilent 244K in accordance with the manufacturer's protocol (Agilent Technologies, Santa Clara, CA, USA). The data were analyzed with the aid of Genomic Workbench 6.5 software (Agilent) and UCSC Human Genome Browser (http://genome.ucsc.edu).

Fluorescence *in situ* hybridization

Fluorescence *in situ* hybridization was performed using standard methods. phytohaemagglutinin-stimulated lymphocytes or Epstein-Barr virus-transformed lymphoblastoid cell lines were arrested by exposure to colcemid. Metaphase preparations were then obtained by hypotonic treatment with 0.075 M KCl followed by methanol/acetate fixation. Bacterial artificial clones on 2q14.3, RP11-11G20 (chr2:126,018,973–126,184,807) and 140B20 (chr2:128,035,141–128,559,312), were used as test probes with a chromosome 2 centromere probe (CEP2 SpectrumOrange Probe; Abbott Laboratories, Abbott Park, IL, USA) used as a reference. The probe was labeled by nick translation with digoxigenin-11-dUTP. After hybridization, the probe was detected with DyLight 488 Anti-Digoxigenin/Digoxin. Chromosomes were visualized by counterstaining with 4',6-diamino-2-phenylindole.

Analysis of junction fragments

To isolate a junction fragment, standard or long-range PCR was performed using LA Taq (TaKaRa, Shiga, Japan). The PCR conditions were 35 cycles of 10 s at 98 °C and 15 min at 60 °C. PCR primers were designed using sequence data from the human genome database. The primers used for amplification were as follows: del2-3F, 5'-GCTTGCTTTGTTCAACACCCTGAG-3' and del2-5R, 5'-TACTTGTTGTCACTTCGTTGGTATTC-3'. PCR products were directly sequenced with the PCR primers using the Sanger method. Breakpoint sequences were characterized using the RepeatMasker (http://www.repeatmasker.org/) and the non-B DB (http://nonb.abcc.ncifcrf.gov/apps/site/default).

RESULTS

Standard cytogenetic evaluations of the study couple revealed a del(2)(q13q14.2) deletion in the women (Figure 1a). As we did not obtain a parental sample, we could not determine whether this was a *de novo* deletion. To demarcate this deletion and attempt to identify the genes responsible for the recurrent pregnancy loss in this female subject, we performed cytogenetic microarray analyses. We, thereby, identified a 2.8-Mb deletion, arr[hg19] 2q14.3(124,622,589–127,367,440)x1 (Figure 1c), which was not found in the public databases such as Human Genome Variation Database (https://gwas.biosciencedbc.jp) and Database of Genomic Variants (http://dgv.tcag.ca/dgv/app/home). It was confirmed by standard fluorescence *in situ* hybridization with a BAC probe to be located at 2q14.3 (Figure 1b). *CNTNAP5* was found to be the only gene in this deleted region. *CNTNAP5* is a brain-specific gene that encodes a protein belonging to the neurexin superfamily of unknown function. The entire *CNTNAP5* gene was lost via the 2.8-Mb deletion. We reevaluated the phenotype of the case and confirmed that the case was a normal healthy female except for the recurrent pregnancy loss. Although some overlapping deletions were identified in the disease-associated structural variant databases such as ISCA (https://www.iscaconsortium.org) and DECIPHER (http://decipher.sanger.ac.uk),

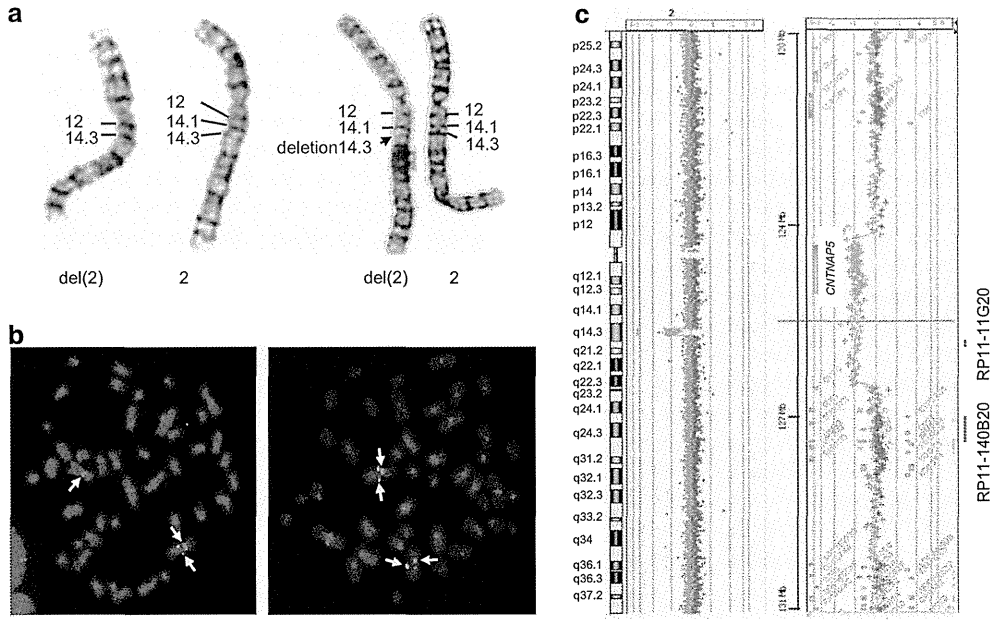

Figure 1 Cytogenetic analyses of the female patient examined in this study. (**a**) Partial karyotype showing a normal chromosome 2 and that with an interstitial deletion. The initial analysis showed the karyotype 46,XX,del(2)(q13q14.2), but the re-evaluation after microarray confirmed 46,XX,del(2)(q14.3q14.3). (**b**) Fluorescence *in situ* hybridization analysis of metaphase chromosomes. The yellow arrows indicate signals corresponding to RP11-11G20 (left, green) or 140B20 (right, green) located at 2q14.3. Red signals indicate the centromere of chromosome 2 (white arrows). RP11-11G20 shows a heterozygous deletion while RP11-140B20 is not deleted. (**c**) Cytogenetic array data. The left panel shows the whole chromosome 2 and the right panel shows the detail. The location of the probes are indicated at the right.

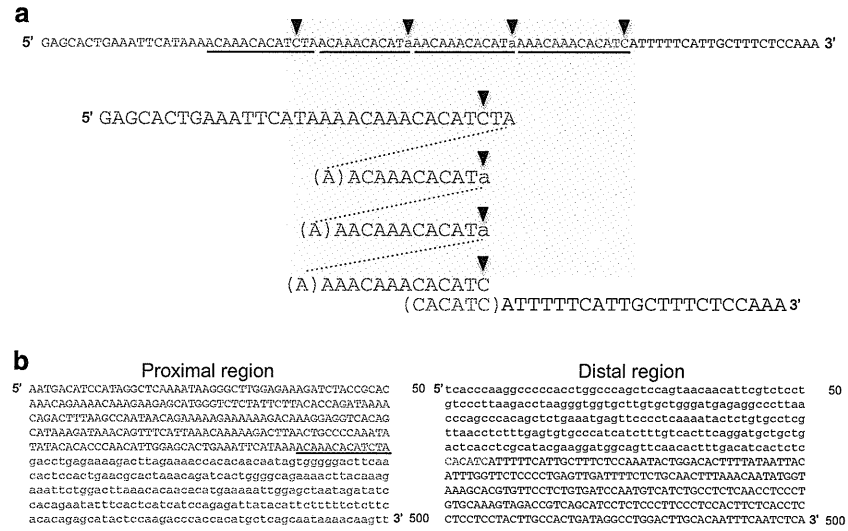

Figure 2 Analyses of the breakpoints and junction of the 2.8-Mb deletion. (**a**) Deletion junction. Nucleotides in blue indicate the sequence of the proximal region, while those in black indicate the distal sequence. The sequences of 11–13-nucleotides repeated four times are underlined. Nucleotides in red or green are those participating in microhomology. Nucleotide positions depicted by arrowheads are occasionally mutated. Those in lowercase are the mutations. (**b**) Sequences of the proximal and distal breakpoint regions. Nucleotides depicted in lowercase are deleted. The six nucleotides in green are those commonly appearing in both proximal and distal regions, and used junction formation as microhomology.

we found no case with a recurrent pregnancy loss. Taken together, these observations led us to the supposition that the deletion might be benign.

To analyze the breakpoint of this deletion at a nucleotide resolution, multiple PCR primers were designed upstream and downstream of the putative breakpoint and long-range PCR was performed using one upstream primer and one downstream primer. One of the PCR primer pairs successfully yielded a PCR product that incorporated the deletion junction. At this junction, we found that a 11–13-nucleotide sequence, originally located at the proximal breakpoint region, was repeated four times with a one-nucleotide microhomology at the junction between each repeat (Figure 2a). Finally, the proximal and distal region was joined with a six-nucleotide microhomology. We found no repeat number variation manifesting as a polymorphism in the general population in the 1000 Genome database (http://www.1000genomes.org). Hence, the four copies of the 11–13-nucleotide repeat were a concurrent by-product of the *de novo* emergence of the 2.8-Mb deletion.

We further analyzed the sequence around the proximal and distal breakpoint regions (Figure 2b). The proximal breakpoint region was located within the LINE1 element, while no characteristic sequence was found around the distal breakpoint. We did not identify any non-B DNA motif that could have potentially induced replication fork stalling at either the proximal or distal breakpoint regions.[11]

DISCUSSION

The female patient suffering from a recurrent pregnancy loss examined in this study was found to carry a 2.8-Mb deletion that included only one gene, *CNTNAP5*. *CNTNAP5* is a brain-specific gene encoding a member of the neurexin superfamily of unknown function. Although the deletion of *CNTNAP5* has been reported in some patients with intellectual disability or autism, the association between this deletion and these disorders is unclear.[12,13] It might be unlikely, however, that the deletion of *CNTNAP5* would affect female reproductive functions and the genetic basis for the recurrent pregnancy loss of our study patient thus remained uncertain. Such a large deletion as seen in our patient can exist without any phenotypic abnormalities if the genes that are contained in the region in question is dispensable. A similar large deletion, del(2)(q13q14.1), has been reported previously in a woman with no phenotypic abnormalities,[14] although this deleted region does not overlap with the one identified in our current study.

Nearly 50% of reported deletions/duplications carry microhomology at the junctions, suggesting that these GCRs are generated via the replication-related pathways fork stalling and template switching or microhomology-mediated break-induced replication.[9] However, these terms are mostly defined on the basis of phenomenological findings of junction sequence. Single-strand nicks that arise before S-phase entry might trigger microhomology-mediated break-induced replication, but the biological evidence for this is still lacking.[8,15] Arlt *et al.*[16] designed an elegant experiment to demonstrate the involvement of replication stress in the generation of GCRs with microhomology. They cultured cells with aphidicolin and successfully induced *de novo* copy number abnormalities including both deletions and duplications. They also analyzed the junctions of these rearrangements and consistently found microhomology, which is analogous to human copy number abnormalities. Further, these rearrangements with microhomology have been observed even in non-homologous end joining-deficient cell lines.[17] These data may represent direct evidence that replication stress can induce microhomology-mediated GCRs.

Strikingly, we found in our current experiments that 11–13-nucleotide stretches were repeated four times at the junction of the deletion in our female subject. This observation is consistent with serial or backward replication slippage that has been proposed previously.[18,19] In addition, the presence of a base substitution at the same nucleotide in the repeats suggests that some modification of the nucleotides that could impede the progression of a replication fork may be a mechanism underlying the onset of the deletion. It has

been reported that several rounds of invasion, extension and dissociation are repeated in the template switching in break-induced replication.[20] In our current case, microhomology was observed not only between each repeat unit but also between the proximal and distal breakpoints, suggesting that a similar mechanism, that is, a microhomology-mediated restart of replication, finally bypassed the replication impediment leading to the deletion. It is possible that the proximal DNA end could invade a distal breakpoint region as far as 2.8 Mb away, as both regions might be in close proximity in the nucleus and be replicated concurrently.

An unresolved question that remained from our current analyses was the nature of the molecular pathway for DNA damage repair that is utilized in the development of replication stress-induced GCR. The presence of base substitutions within the nascent repeat sequence commonly observed in serial replication slippage might provide clues toward identifying this pathway.[18,19] When the replication fork encounters a damaged base or nucleotide in a leading-strand template, the damaged lesion would generally be bypassed in a homology-dependent manner using a nascent sister chromatid originating from the lagging-strand. However, in case rad51 is unavailable or in short supply, error-prone translesion synthesis or error-free pathways based on replication fork regression and template switching by forming a chicken-foot structure would be activated. These pathways are mediated by monoubiquitination or poly-ubiquitination of proliferating cell nuclear antigen, respectively and are referred to as post-replication repair.[21,22] The error-prone translesion synthesis pathway is usually suppressed but another possible mechanism is the error-prone restart of DNA replication proposed recently.[23] When the replication fork stalls at sites of DNA damage, the microhomology-primed restart would be error prone possibly mediated by a DNA polymerase with low-processivity. Increased mutation rates during the replication of repeat regions might result from a similar mechanism.[24,25]

In conclusion, our current analysis of a female patient with recurrent pregnancy loss implicates the post-replication repair pathway as a mechanism underlying copy number variation in mammals. A full elucidation of the molecular pathway leading to serial/backward replication slippage deserves further investigation.

CONFLICT OF INTEREST

The authors declare no conflict of interest.

ACKNOWLEDGEMENTS

We thank Dr Hiroshi Kogo and Dr Makiko Tsutsumi for helpful discussions and Mrs Narumi Kamiya for technical assistance. These studies were supported by a grant-in-aid for Scientific Research from the Ministry of Education, Culture, Sports, Science and Technology of Japan (21390101 and 24390085) and from the Ministry of Health, Labour and Welfare of Japan (10103465) to HK

1 Beckmann, J. S., Estivill, X. & Antonarakis, S. E. Copy number variants and genetic traits: closer to the resolution of phenotypic to genotypic variability. *Nat. Rev. Genet.* **8,** 639–646 (2007).
2 Kurahashi, H., Bolor, H., Kato, T., Kogo, H., Tsutsumi, M., Inagaki, H. *et al.* Recent advance in our understanding of the molecular nature of chromosomal abnormalities. *J. Hum. Genet.* **54,** 253–260 (2009).
3 Shaikh, T. H., Kurahashi, H. & Emanuel, B. S. Evolutionarily conserved low copy repeats (LCRs) in 22q11 mediate deletions, duplications, translocations, and genomic instability: an update and literature review. *Genet. Med.* **3,** 6–13 (2001).
4 Stankiewicz, P. & Lupski, J. R. Genome architecture, rearrangements and genomic disorders. *Trends Genet.* **18,** 74–82 (2002).
5 Baumer, A., Dutly, F., Balmer, D., Riegel, M., Tükel, T., Krajewska-Walasek, M. *et al.* High level of unequal meiotic crossovers at the origin of the 22q11. 2 and 7q11.23 deletions. *Hum. Mol. Genet.* **7,** 887–894 (1998).
6 Chapman, J. R., Taylor, M. R. & Boulton, S. J. Playing the end game: DNA double-strand break repair pathway choice. *Mol. Cell.* **47,** 497–510 (2012).
7 Lee, J. A., Carvalho, C. M. & Lupski, J. R. A DNA replication mechanism for generating nonrecurrent rearrangements associated with genomic disorders. *Cell* **131,** 1235–1247 (2007).
8 Hastings, P. J., Lupski, J. R., Rosenberg, S. M. & Ira, G. Mechanisms of change in gene copy number. *Nat. Rev. Genet.* **10,** 551–564 (2009).
9 Conrad, D. F., Bird, C., Blackburne, B., Lindsay, S., Mamanova, L., Lee, C. *et al.* Mutation spectrum revealed by breakpoint sequencing of human germline CNVs. *Nat. Genet.* **42,** 385–391 (2010).
10 Kidd, J. M., Graves, T., Newman, T. L., Fulton, R., Hayden, H. S., Malig, M. *et al.* A human genome structural variation sequencing resource reveals insights into mutational mechanisms. *Cell* **143,** 837–847 (2010).
11 Cer, R. Z., Donohue, D. E., Mudunuri, U. S., Temiz, N. A., Loss, M. A., Starner, N. J. *et al.* Non-B DB v2.0: a database of predicted non-B DNA-forming motifs and its associated tools. *Nucleic. Acids. Res.* **41,** D94–D100 (2013).
12 Ballarati, L., Recalcati, M. P., Bedeschi, M. F., Lalatta, F., Valtorta, C., Bellini, M. *et al.* Cytogenetic, FISH and array-CGH characterization of a complex chromosomal rearrangement carried by a mentally and language impaired patient. *Eur. J. Med. Genet.* **52,** 218–223 (2009).
13 Pagnamenta, A. T., Bacchelli, E., de Jonge, M. V., Mirza, G., Scerri, T. S., Minopoli, F. *et al.* Characterization of a family with rare deletions in CNTNAP5 and DOCK4 suggests novel risk loci for autism and dyslexia. *Biol. Psychiatry* **68,** 320–328 (2010).
14 Sumption, N. D. & Barber, J. C. A transmitted deletion of 2q13 to 2q14.1 causes no phenotypic abnormalities. *J. Med. Genet.* **38,** 125–127 (2001).
15 Hastings, P. J., Ira, G. & Lupski, J. R. A microhomology-mediated break-induced replication model for the origin of human copy number variation. *PLoS Genet.* **5,** e1000327 (2009).
16 Arlt, M. F., Mulle, J. G., Schaibley, V. M., Ragland, R. L., Durkin, S. G., Warren, S. T. *et al.* Replication stress induces genome-wide copy number changes in human cells that resemble polymorphic and pathogenic variants. *Am. J. Hum. Genet.* **84,** 339–350 (2009).
17 Arlt, M. F., Rajendran, S., Birkeland, S. R., Wilson, T. E. & Glover, T. W. *De novo* CNV formation in mouse embryonic stem cells occurs in the absence of Xrcc4-dependent nonhomologous end joining. *PLoS Genet.* **8,** e1002981 (2012).
18 Chen, J. M., Chuzhanova, N., Stenson, P. D., Férec, C. & Cooper, D. N. Meta-analysis of gross insertions causing human genetic disease: novel mutational mechanisms and the role of replication slippage. *Hum. Mutat.* **25,** 207–221 (2005).
19 Chen, J. M., Chuzhanova, N., Stenson, P. D., Férec, C. & Cooper, D. N. Complex gene rearrangements caused by serial replication slippage. *Hum. Mutat.* **26,** 125–134 (2005).
20 Smith, C. E., Llorente, B. & Symington, L. S. Template switching during break-induced replication. *Nature* **447,** 102–105 (2007).
21 Daigaku, Y., Davies, A. A. & Ulrich, H. D. Ubiquitin-dependent DNA damage bypass is separable from genome replication. *Nature* **465,** 951–955 (2010).
22 Ulrich, H. D. & Walden, H. Ubiquitin signalling in DNA replication and repair. *Nat. Rev. Mol. Cell Biol.* **11,** 479–489 (2010).
23 Mizuno, K., Miyabe, I., Schalbetter, S. A., Carr, A. M. & Murray, J. M. Recombination-restarted replication makes inverted chromosome fusions at inverted repeats. *Nature* **493,** 246–249 (2013).
24 Shah, K. A., Shishkin, A. A., Voineagu, I., Pavlov, Y. I., Shcherbakova, P. V. & Mirkin, S. M. Role of DNA polymerases in repeat-mediated genome instability. *Cell Rep.* **2,** 1088–1095 (2012).
25 Saini, N., Zhang, Y., Nishida, Y., Sheng, Z., Choudhury, S., Mieczkowski, P. *et al.* Fragile DNA motifs trigger mutagenesis at distant chromosomal loci in *Saccharomyces cerevisiae*. *PLoS Genet.* **9,** e1003551 (2013).

Mishra et al. Molecular Cytogenetics 2014, 7:55
http://www.molecularcytogenetics.org/content/7/1/55

MOLECULAR CYTOGENETICS

RESEARCH Open Access

Breakpoint analysis of the recurrent constitutional t(8;22)(q24.13;q11.21) translocation

Divya Mishra[1†], Takema Kato[1†], Hidehito Inagaki[1], Tomoki Kosho[2], Keiko Wakui[2], Yasuhiro Kido[3], Satoru Sakazume[3], Mariko Taniguchi-Ikeda[4], Naoya Morisada[4], Kazumoto Iijima[4], Yoshimitsu Fukushima[2], Beverly S Emanuel[5,6] and Hiroki Kurahashi[1*]

Abstract

Backgrounds: The t(8;22)(q24.13;q11.2) has been identified as one of several recurrent constitutional translocations mediated by palindromic AT-rich repeats (PATRRs). Although the breakage on 22q11 utilizes the same PATRR as that of the more prevalent constitutional t(11;22)(q23;q11.2), the breakpoint region on 8q24 has not been elucidated in detail since the analysis of palindromic sequence is technically challenging.

Results: In this study, the entire 8q24 breakpoint region has been resolved by next generation sequencing. Eight polymorphic alleles were identified and compared with the junction sequences of previous and two recently identified t(8;22) cases . All of the breakpoints were found to be within the PATRRs on chromosomes 8 and 22 (PATRR8 and PATRR22), but the locations were different among cases at the level of nucleotide resolution. The translocations were always found to arise on symmetric PATRR8 alleles with breakpoints at the center of symmetry. The translocation junction is often accompanied by symmetric deletions at the center of both PATRRs. Rejoining occurs with minimal homology between the translocation partners. Remarkably, comparison of der (8) to der(22) sequences shows identical breakpoint junctions between them, which likely represent products of two independent events on the basis of a classical model.

Conclusions: Our data suggest the hypothesis that interactions between the two PATRRs prior to the translocation event might trigger illegitimate recombination resulting in the recurrent palindrome-mediated translocation.

Keywords: PATRR, t(8;22), Palindrome-mediated translocation, Supernumerary der(8)t(8;22)

Background

The constitutional t(8;22)(q24.13;q11.2) is recognized as a one of several recurrent translocations in humans [1]. The most prevalent recurrent constitutional translocation is the t(11;22)(q23;q11) [2]. Although t(11;22) balanced-translocation carriers are phenotypically normal, they often manifest problems with reproduction such as infertility, recurrent pregnancy loss, or the birth of unbalanced offspring with the supernumerary der(22)t(11;22) syndrome (Emanuel syndrome [MIM 609029]) [3]. Among the small supernumerary marker chromosomes seen clinically, +der(22)t(11;22) is the most frequent, while + der (22)t(8;22) is the second most prevalent [4]. Similar to the t(11;22), balanced carriers of the t(8;22) are often identified after the birth of an unbalanced offspring with the supernumerary der(22) t(8;22), the phenotype of which includes extremity anomalies, mild dysmorphism and intellectual disability.

The mechanism that leads to the constitutional t(11;22) (q23;q11) has been extensively studied. The breakpoints of both chromosomes are consistently located within palindromic AT-rich repeats (PATRRs) [5-9]. Palindromic regions, i.e. inverted repeats, have a potential for the formation of hairpin/cruciform structures by intrastrand annealing and palindrome induced genomic instability has been demonstrated in many experimental model organisms [10-12]. In humans, a considerable number of *de novo* t(11;22)s arise during spermatogenesis, but *de novo* occurrences have not been detected in tissues other than sperm [13]. It has been proposed that the secondary

* Correspondence: kura@fujita-hu.ac.jp
†Equal contributors
[1]Division of Molecular Genetics, Institute for Comprehensive Medical Science, Fujita Health University, Toyoake, Aichi 470-1192, Japan
Full list of author information is available at the end of the article

structure of the palindromic DNA during spermatogenesis induces genomic instability leading to the recurrent chromosomal translocation [14,15]. Taking advantage of breakpoint co-localization on 22q11, the translocation junction fragments of the t(8;22) have been isolated, the breakpoints on 8q24 were assessed, and a similar mechanism of translocation was suggested [1,16]. Although PATRR-like sequence (PATRR8) was compiled from the junction sequences, detailed analysis of the breakpoint region have not been performed since the analysis of the palindromic region is technically challenging [17]. Further, since the database of human reference sequence does not include the complete sequence of PATRR8, details of the t(8;22) translocation mechanism are incomplete.

In this study, we first obtained the complete sequence of several polymorphic PATRR8 alleles from normal individuals using next generation sequencing. Using translocation-specific PCR, we also determined the translocation junctions in two unrelated Japanese families with the t(8;22)(q24.13;q11.2). We performed an investigation to examine the breakpoint within PATRR8 and PATRR22 by comparing the junction sequences with the normal PATRR8 and PATRR22. These data further confirm that the t(8;22) translocation is a recurrent rearrangement with a mechanism consistent with that proposed for the t(11;22) and the t(8;22) in previous studies. These findings provide additional support for the role of palindromic sequences in genomic instability. Further, our new finding, the similarity of the der(8) and the der(22) sequences, might elicit a new feature of palindrome-mediated translocations.

Results

Genomic structure of the PATRR8

Based on the putative PATRR8 sequences compiled by analysis of translocation junctions, the majority of PATRR8 is deleted and only a portion of the proximal arm appears in the human genome database [1]. To determine the complete sequence of PATRR8, we first attempted conventional PCR followed by standard Sanger sequencing. The sizes of the PCR products that include PATRR8 vary among individuals. We previously classified them into four categories: long (L), medium (M), short (S) and super-short (SS) [1]. The M and S alleles were the major alleles, while L and SS alleles were less frequent. Despite the fact that we could generate the complete sequence of the SS allele, their AT-rich and palindromic nature prevented us from sequencing the central region of the PATRR in other allele types [17].

Next, we attempted to sequence the PCR product by massively parallel sequencing using a next generation sequencer. Although the central region was under-represented (~50 reads out of ~30,000 reads per PCR product), we finally obtained the sequence of the entire PATRR8 in 11 out of 24 PCR products. Indeed, the sequence data obtained by next generation sequencing demonstrated that size polymorphisms of the PCR products result from size polymorphisms of PATRR8 itself as well as size variation in the flanking AT-rich repeat region (Figure 1A, Additional file 1: Figure S1).

The M allele (~350 bp), one of the most frequent variants, manifests a nearly perfect palindrome (Table 1). AT-richness is as high as 98%. Identity between the proximal and distal arms is >98%, showing a nearly perfect palindromic structure. Subtle nucleotide alterations produce three subtypes, M1, M2 and M3 (Figure 1B). The S allele (~310 bp), the other most frequent variant, also manifests a high AT-content (97%) and a perfect palindrome (identity 100%). The L allele (423 bp) and the SS allele (98 bp) are less frequent. The SS allele appears to be an asymmetrically deleted version of the S allele, whereas the L allele appears to have an asymmetric insertion of AT-rich sequence of unknown origin. The PATRR8 sequence appearing in the human genome database was not found to be a subtype of PATRR8 polymorphism. The deletion in the database carries a 16 bp homology at the junction (Additional file 1: Figure S1), suggesting that the sequence is an artifact generated during bacterial culture for clone preparation for sequencing.

Unlike other translocation-related PATRRs, PATRR8 has another AT-rich flanking region both at its proximal and distal side. Both of these AT-rich regions manifest size polymorphisms. The proximal flanking region carries a 35 bp direct repeat, whose copy number is increased in M alleles (Additional file 1: Figure S1). The distal region also carries a similar 28 bp direct repeat, copy number variation of which produces size polymorphism. Since we could not distinguish between M and S alleles simply by gel electrophoresis due to these size polymorphisms in the flanking regions, we could not determine the exact frequency of polymorphic PATRR8 alleles in the general population.

Analysis of the breakpoints of the der(8) and der(22)

Using primers flanking PATRR8 and PATRR22 (Figure 2A), genomic DNAs from all of the t(8;22) cases yielded translocation specific PCR products (Figure 2B). Approximately 850 bp of the der(8) and 650 bp of the der(22) harboring the translocation junction were amplified by PCR from balanced translocation carriers in family 1 (FHU13-033) and family 2 (FHU13-027) as well as from the unrelated balanced translocation carriers published previously [1]. Only the der(22) PCR product was amplified from the proband in family 1 (FHU13-031) with the typical supernumerary der(22)t(8;22). Now that we have the complete sequence of PATRR8, we can compare the junction sequences with the putative original sequences. Based on sequence polymorphisms at the center and on the arm regions of PATRR8, we can deduce the original allele types.

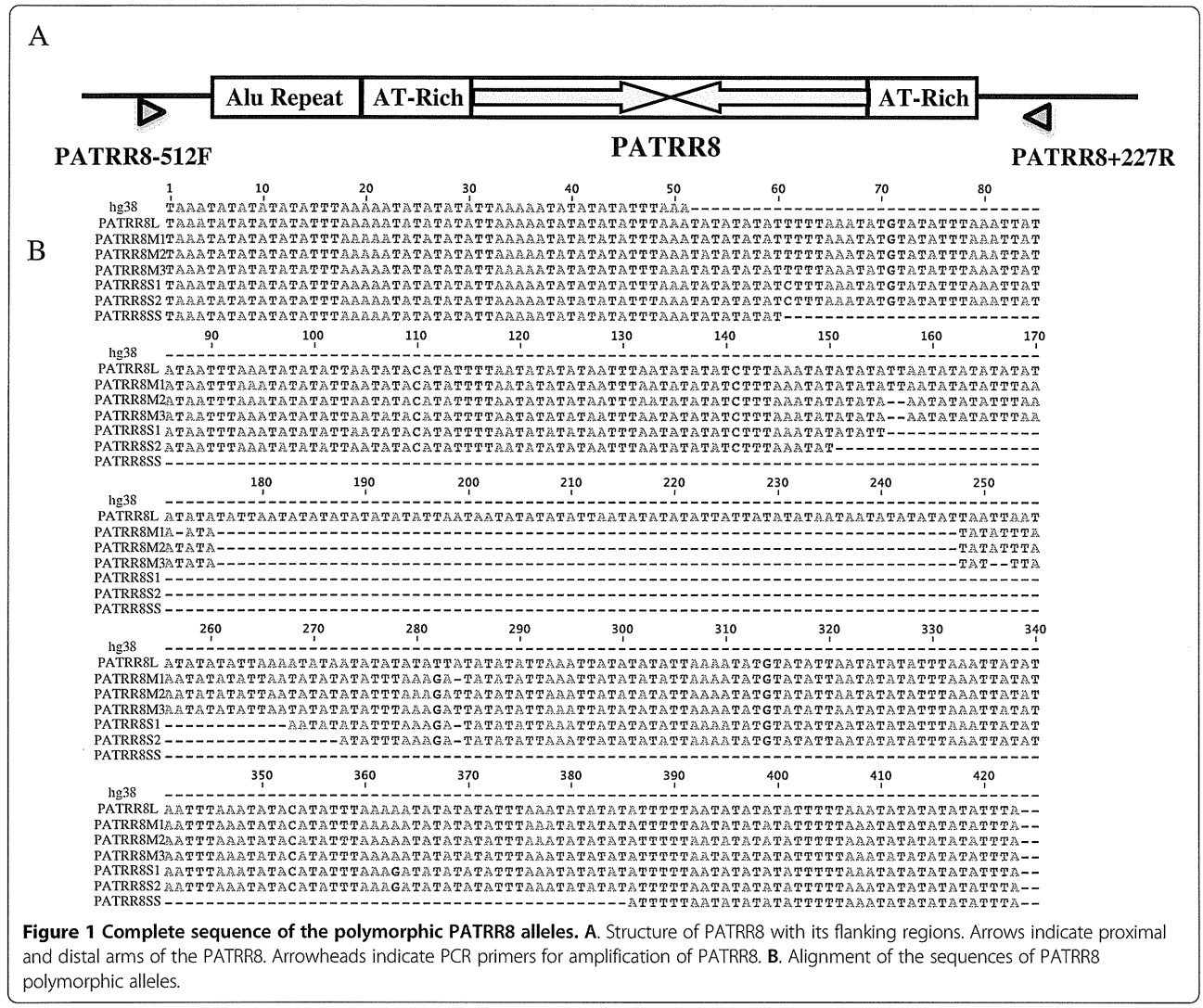

Figure 1 Complete sequence of the polymorphic PATRR8 alleles. A. Structure of PATRR8 with its flanking regions. Arrows indicate proximal and distal arms of the PATRR8. Arrowheads indicate PCR primers for amplification of PATRR8. **B**. Alignment of the sequences of PATRR8 polymorphic alleles.

We suggest that FHU13-033 (family 1) as well as case 13 originated from PATRR8M, while FHU13-027 (family 2) as well as cases 8, 9, 12 and 16 originated from PATRR8S1 (Table 2). Regarding the PATRR22, FHU13-033 (family 1) and FHU13-027 (family 2) originated from PATRR22C, while cases 12 and 13 originated from PATRR22A. PATRR22 sequence in case 16 was so diverged from known PATRR22 variants that we could not determine the origin. Virtually all of the translocations occurred on symmetrical alleles of PATRR8 and PATRR22.

When the chromosome 8 portions of the der(8) and der(22) were aligned with PATRR8, the central region

Table 1 Characterization of the polymorphic PATRR8 alleles

Allele	Size (bp)	AT content (%)	%Identity*	ΔG (kcal/mol)	Accession no
PATRR8L	423	99%	92.7%	-142.71	AB968359
PATRR8M1	349	98%	99.4%	-139.20	AB968360
PATRR8M2	349	98%	98.3%	-132.12	AB968361
PATRR8M3	347	98%	98.3%	-131.36	AB968362
PATRR8S1	310	97%	100%	-125.90	AB968363
PATRR8S2	300	97%	100%	-122.22	AB968364
PATRR8SS	98	98%	96.0%	-33.22	AB969308

*%identity (similarity) between proximal and distal arms.

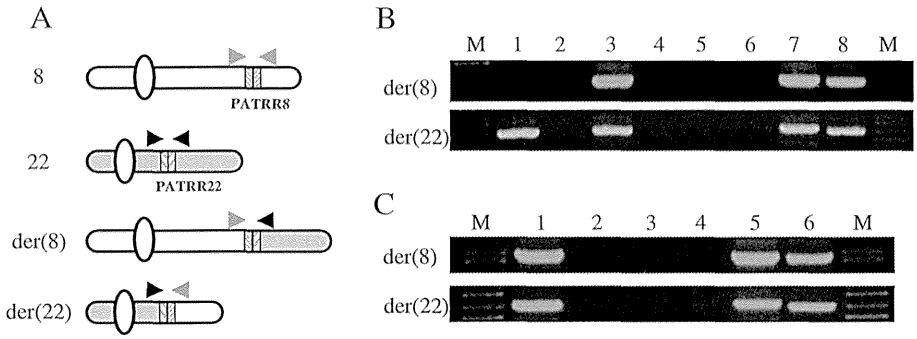

Figure 2 The der(8) and the der(22) junction fragments of the t(8;22). A. Diagram for the translocation-specific PCR system. Chromosome 8 is indicated in white, while chromosome 22 is depicted in grey. Hatched boxes indicate PATRR arms. Translocation-specific PCR was performed with one primer designed at the flanking region of PATRR8 (grey primers) and with the other primer at the flanking region of PATRR22 (black primers). **B**. Results of family 1. Upper panel indicates results for the der(8), while lower panel indicates those of the der(22). Lane M, size markers; lane 1, FHU13-031 (proband); lane 2, FHU13-032 (father); lane 3, FHU13-033 (mother); lanes 4 and 5, normal healthy controls; lane 6, water control; lanes 7 and 8, balanced t(8;22) translocation carriers unrelated to the family. **C**. Results of family 2. Lane M, size markers; lane 1, FHU13-027 (proband); lanes 2 and 3, normal healthy controls; lane 4, water control; lanes 5 and 6, balanced t(8;22) translocation carriers unrelated to the family.

often appeared to be deleted (Figure 3A). Although the extent of deletion differs amongst cases, the sequence derived from the proximal and the distal arms shows loss of the same number of nucleotides from PATRR8. Likewise, the deletion is symmetrically located at the center of PATRR22 (Figure 3B). This suggests that the breakage always occurred at the center of the palindrome followed by a progression of bidirectional deletion.

Analyses of the junctions of the der(8) and der(22)

We analyzed the junctions of PATRR8 and PATRR22 both for the der(8) and der(22). No substantial homology could be observed between PATRR8 and PATRR22 (35-50% similarity). We only observed a few identical nucleotides at the point where the original PATRR8 and PATRR22 sequences were joined (2-11 bp) (Figure 3A, B). Both PATRR8 and PATRR22 are so highly AT-rich that even homology-independent rejoining could manifest some microhomology at the junction by chance [9]. Therefore, the molecular pathways that are assumed to drive generation of this translocation might include microhomology-mediated end joining, classical non-homologous end joining, or alternative non-homologous end joining.

Comparison between the der(8) and der(22) sequences

We further compared the junction sequences of the der (8) and the der(22). Strikingly, the der(8) and the der(22) sequences were identical at the junctions in all cases (Figure 4), although subtle nucleotide differences were identified in the arm region that reflected nucleotide differences between the proximal and distal arms. On the basis of a standard mechanism of translocation formation based on double-strand DNA repair, formation of the der(8) and the der(22) occur independently [18]. If there were a long stretch of homologous sequence at the junction, there would be a chance to produce the same junction fragments independently. However, even at the junction with microhomology of only a few nucleotides, the der(8) and the der(22) sequences were identical.

Table 2 Origin of the PATRR subtypes

Sample name	PATRR8	PATRR22	Reference
Family 1(FHU13-033)	PATRR8M	PATRR22C	This study
Family 2 (FHU13-027)	PATRR8S1	PATRR22C	This study
Case 8*	PATRR8S1	ND**	Sheridan et al. 2010 [1]
Case 9*	PATRR8S1	ND**	Sheridan et al. 2010 [1]
Case 12 (CH00-180)	PATRR8S1	PATRR22A	This study (Sheridan et al. 2010) [1]
Case 13 (CH07-194)	PATRR8M	PATRR22A	This study (Sheridan et al. 2010) [1]
Case 16	PATRR8S1	NA***	Sheridan et al. 2010 [1]

*Only the der(22) was analyzed.
**Not determined, ***Not applicable.

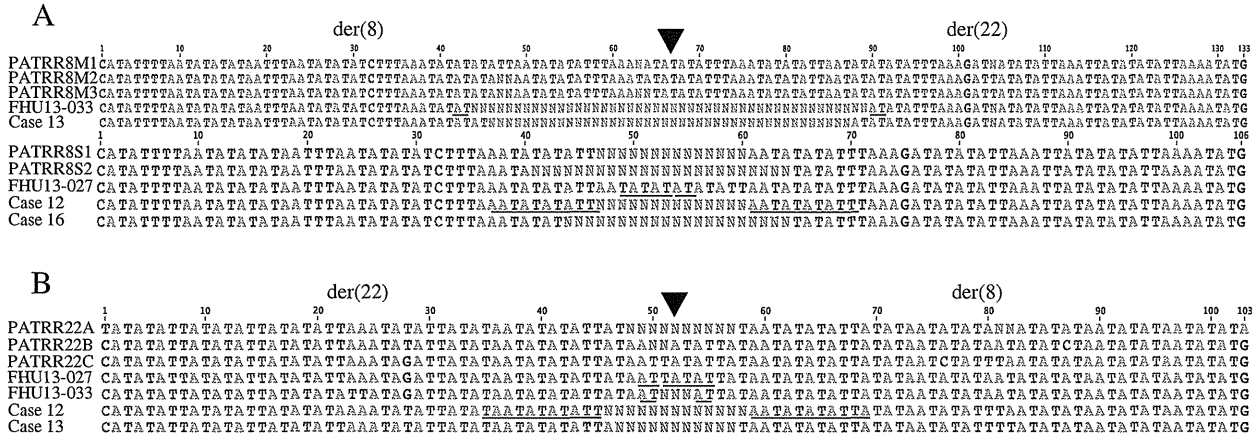

Figure 3 Sequence comparison between the der(8) and the der(22) junction fragments with the putative original PATRRs. A. Compilation of the chromosome 8 side of the der(8) and der(22) with the PATRR8. **B**. Compilation of the chromosome 22 side of the der(8) and der(22) with the PATRR22. Triangles indicate the center of the PATRRs. Nucleotides participating in microhomology are underlined.

Discussion

Characterization of the PATRR8

In this study, we determined the entire PATRR8 sequence in humans for the first time. All of the translocation-related PATRRs identified to date have three common features. 1) They comprise nearly perfect palindromes, whose lengths are several hundred base pairs. 2) An AT-rich region is located at the center, while there are relatively non-AT-rich regions at both ends. 3) Another AT-rich region exists flanking the PATRR [9]. Although non-AT-rich regions were absent within PATRR8, it possesses all three common features of translocation related PATRRs. It is proposed that all of these features foster the propensity for forming secondary structure at palindromic regions. Indeed, PATRR8 contributes to generation of not only the t(8;22), but also the constitutional t(3;8) that is associated with hereditary renal cell carcinoma predisposition, suggesting that the PATRR8 is a hotspot for palindrome-mediated translocations [19]. It is likely that for the t(8;22), as for other PATRR-related recurrent translocations such as the t (11;22) and t(17;22), DNA secondary structure might contribute to the generation of the translocation.

Similar to other translocation-related PATRRs, PATRR8 manifests size polymorphisms due to those within the PATRR itself as well as those in the flanking AT-rich

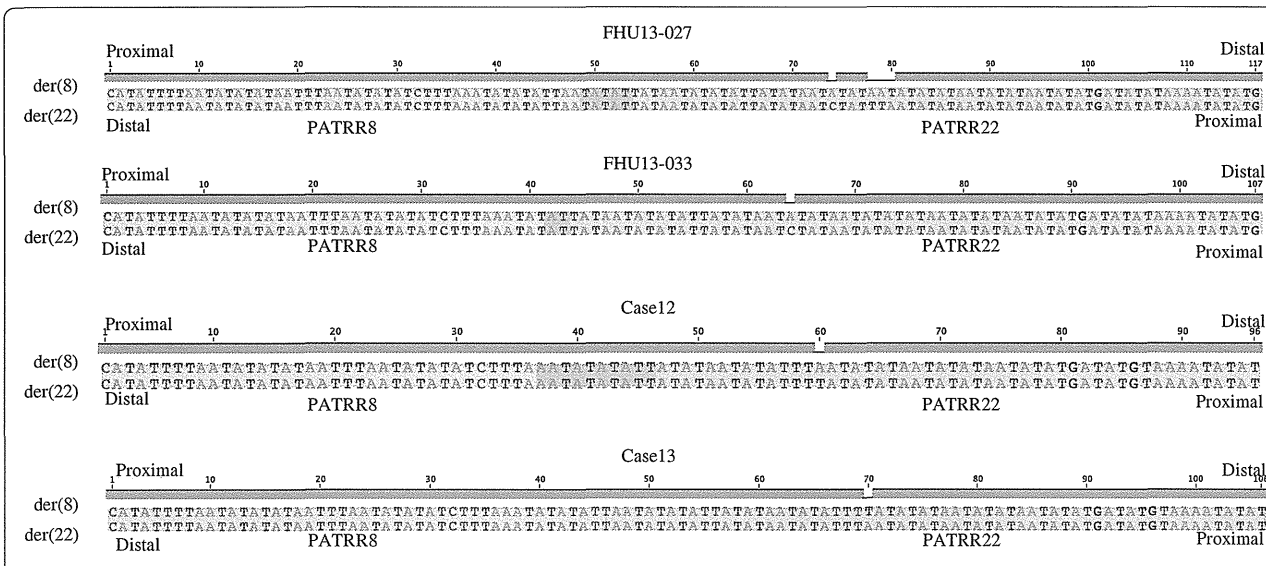

Figure 4 Sequence comparison between der(8) and the der(22) junction fragments in each case. Sequences are shown from PATRR8 side (blue) to the PATRR22 side (pink). Nucleotides participating in microhomology are shown in purple.

region. Although minor variations are present at the nucleotide level, size variations of PATRR8 were found to be of only four types; two symmetric types and two asymmetric types. This might imply that PATRR8 is generally transmitted stably and is not predisposed to insertion or deletion. Alternatively, it is possible that PATRR8 might have emerged recently during evolution. Similar to other recurrent PATRR-mediated translocations, the t(8;22) was found to arise from symmetric variants [20,21]. This indirectly but strongly suggests that PATRR8 adopts secondary structures *in vivo*.

Clinical significance for translocation-specific PCR

In all cases, both translocation breakpoints are located within several hundred base pair intervals on each chromosome, which could be identified with primers flanking PATRR8 and PATRR22. Similar to the t(11;22), this translocation-specific PCR is diagnostic since it can detect all of the t(8;22) translocations [22]. For example, in examination of a case like FHU13-027 with a balanced t(8;22) with intellectual disability and mild dysmorphic features, it might be difficult to know if the t(8;22) translocation is responsible for the phenotype as a result of breakpoint variation. On the basis of positive t(8;22)-specific PCR for both derivatives, we could conclude that the case is a standard t(8;22) balanced carrier and the t(8;22) translocation itself was unlikely to be the cause of the phenotype. Such translocation-specific PCR can also be useful in determining the origin of a small supernumerary marker chromosome of unknown origin. Since the t(8;22) is the second most frequent amongst small supernumerary marker chromosomes [4], t(8;22)-specific PCR is a simple and cost-effective method for marker identification as compared to multicolor spectral karyotyping for example.

Among the conceptions with unbalanced translocation products from a balanced t(8;22) translocation carrier that might result in early pregnancy loss, only a fetus with + der(22) karyotype through meiotic 3:1 segregation might be viable. Prenatal diagnosis for supernumerary der(22)t(8;22) syndrome could be performed via chorionic villus biopsy or amniocentesis. Non-invasive prenatal testing might also be possible, particularly if the male partner is a balanced translocation carrier. Further, translocation-specific PCR can also be applied for pre-implantation diagnosis using DNA amplified by whole genome amplification methods using the genomic DNA from a blastomere or blastocyst biopsy.

Possible mechanism for palindrome-mediated translocation

PATRR-mediated genomic instability is likely to occur via two distinct mechanisms; replication-dependent and replication-independent [23,24]. The replication-dependent route is induced by replication fork stalling as a result of a hairpin structure within the lagging-strand template during DNA replication [25]. This is followed by template switching via microhomology leading to gross chromosomal rearrangements like translocations [26] Indeed, this kind of somatic rearrangement is often identified in cancer cells [27]. However, translocation-specific PCR only detects the t(8;22) as well as the t(11;22) in sperm, suggesting that PATRR-mediated translocations arise in gametogenesis, most notably spermatogenesis [13,28]. One of the explanations for spermatogenesis-specific palindrome-mediated genomic instability is that during spermatogenesis a significant number of DNA replications take place. This would be a pre-meiosis hypothesis [2,29]. Indeed, PATRR17 located within an intron of the NF1 gene contributes to some germ-line gross chromosomal rearrangements such as deletions and translocations resulting in neurofibromatosis type 1 [30]. The breakpoint features of these rearrangements are distinct from PATRR-mediated translocations [31,32].

An alternative hypothesis is a post-meiosis hypothesis, which is based on replication-independent cruciform structure formation at the PATRRs by free negative supercoiling induced by extensive histone removal during late spermatogenesis. Symmetrical deletions on both the proximal and distal arms might imply that the deletions do not occur after DNA breakage at the central region of the PATRR followed by dissociation of the proximal and distal arms. Perhaps they occur after the central breakage with the PATRR maintaining its secondary structure, upon annealing of the proximal and distal arms. The symmetrical deletions are reflected in the identical nature of the der(8) and the der(22) sequences, which must be generated as independent events based on a classical DSB repair model for translocation formation [18]. The identical sequence of the der(8) and the der(22) might imply that rejoining occurs between the PATRRs while still keeping their secondary structure. Finally, the partner chromosome of a PATRR-mediated translocation is always another PATRR [2]. Thus, the hairpin-hairpin model proposed by Inagaki et al. might represent a plausible model for PATRR-mediated translocations in humans [33].

Conclusions

In our current study, comparison of der(8) to der(22) sequences shows identical breakpoint junctions between them, which likely represent products of two independent events on the basis of a classical model. Our data suggest the hypothesis that interactions between the two PATRRs prior to the translocation event might trigger illegitimate recombination resulting in the recurrent palindrome-mediated translocation.

Methods

Human samples

In this study, we used genomic DNA samples from cases 12 (CH00-180) and 13 (CH07-194) from the previous study [1]. In addition, we identified two new families of Japanese origin with the t(8;22)(q24;q11) translocation (Figure 5). One family (family 1) was identified through a female proband (FHU13-031) with typical features of the supernumerary der(22)t(8;22) syndrome characterized by clinodactyly, mild dysmorphia with preauricular pit, and intellectual disability. Her normal healthy mother was a balanced t(8;22) translocation carrier (FHU13-033). The other family (family 2) was identified by a female proband who was a balanced t(8;22) translocation carrier (FHU13-027) revealed by screening based upon intellectual disability and mild dysmorphia. The normal healthy mother also carried the same translocation. After informed consent was obtained, peripheral blood samples were obtained. This study was approved by the Ethical Review Board for Human Genome Studies at Fujita Health University (Accession number 145, approved on 16 April 2013).

Next generation sequencing

Genomic DNA was purified by QuickGene-610 L (Fuji Film). PATRR8 was amplified with primers flanking PATRR. PATRR8-512 F (5′-GATTACATATGGCATCT GGTAGGCTG-3′) was used as the forward primer and PATRR8 + 227R (5′-GTGCCAAAATGTCAAGTCATCT GTG-3′) was used as the reverse primer. PCR was performed with the KAPA Extra (KAPA Biosystems). The PCR products were separated by 2% agarose gel electrophoresis and the genotypes for size polymorphism were determined.

To obtain the entire PATRR8 sequence, we used five t (8;22) balanced translocation carriers, who carry only one copy of the intact PATRR8. In addition, we selected 19 normal healthy donors who were heterozygous for size polymorphisms of PATRR8. The PCR products were separated by 2% agarose gel electrophoresis and each PCR product derived from a different allele was purified separately.

For next generation sequencing, tagmentation were performed using a Nextera XT DNA sample prep kit (Illumina) according to the manufacturer's specifications. The libraries were amplified using the KAPA Library Amplification Kit (KAPA Biosystems) with the Nextera Index Kit to add indices and common adapters for subsequent cluster generation and sequencing. Prior to cluster generation, normalized libraries were further quantified by Qubit (Invitrogen Q32866) using the Qubit dsDNA HS Assay Kit (Invitrogen Q32851) and the 2100 Bioanalyzer (Agilent Technologies) using the High Sensitivity DNA Kit (Agilent Technologies, 5067–4626). PhiX control was added to the reaction to increase sequence diversity. Finally, the prepared library was loaded on an Illumina MiSeq clamshell style cartridge for paired end sequencing (Illumina). The data were analyzed using CLC Genomics Workbench. After trimming, reads were assembled as *de novo* assemblies or they were mapped to putative references prepared from junction fragments derived from t(8:22) translocation carriers to produce consensus sequences. Identity was calculated by Emboss Needle software, while ΔG was calculated by mfold.

PCR amplification of the junction fragments

To amplify an ~850 bp product containing the der(8) breakpoint junction fragment and to amplify the ~650 bp product containing the der(22) breakpoint junction fragment, a two-step PCR system was used [17]. The der (8) products were amplified with PATRR8-512 F and PATRR22 + 178R (5′-CATGATTCTGGATAACTTCCA AA-3′) or JF22 (5′-CCTCCAACGGATCCATACT-3′) primers, while the der(22) products were amplified with PATRR8 + 227R and PATRR22-394 F (5′-TCAGTT TATTCCCAAACTCCCAAAT-3′) or JF22 primers. PCRs were performed using LA Taq DNA Polymerase (Takara) and the PCR conditions were as follows: 94°C for 2 min,

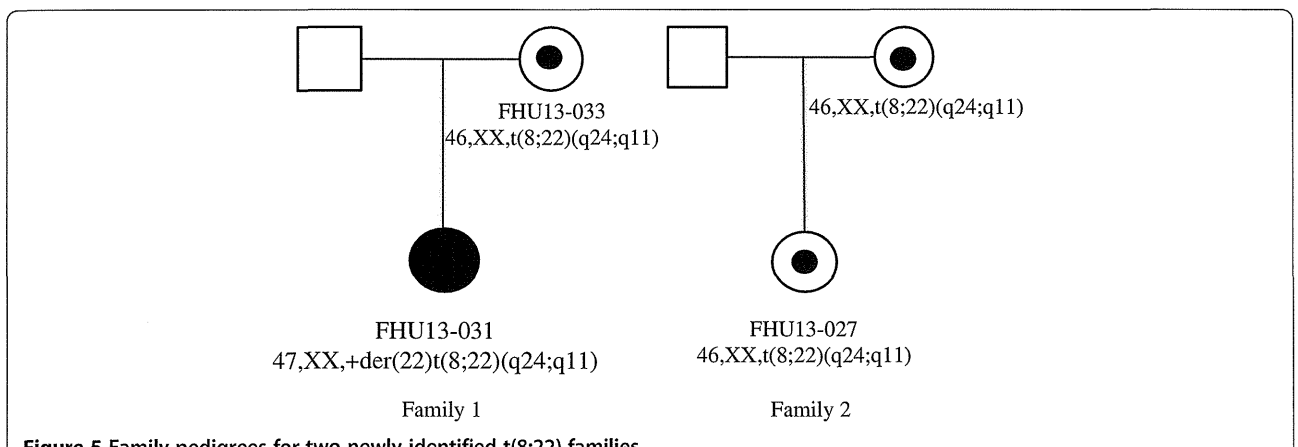

Figure 5 Family pedigrees for two newly identified t(8;22) families.

followed by 35 cycles of 98°C for 30 s, 60°C for 5 min. The resulting PCR products were checked on 2% agarose gels, subjected to ExoSAP-IT digestion (Affymetrix), and then sequenced bidirectionally by capillary electrophoresis (ABI3730 Genetic Analyzer, Applied Biosytems). Sequences were analyzed with Clustalw2, which was used to align the resulting sequences.

Additional file

Additional file 1: Figure S1. Complete sequence of the polymorphic PATRR8 with flanking regions. Large arrows indicate the proximal and distal PATRR arms. Direct repeats at the flanking regions proximal and distal to the PATRR8 are underlined (blue solid or dotted lines). The black lines indicate homology between the proximal and distal region to the PATRR8 deletion that appears in the human genome database.

Competing interests
The authors declare that they have no competing interests.

Authors' contributions
DM - Participated in the design of the study, carried out the molecular biology work, and drafted the manuscript. TKA - Participated in the design of the study, carried out the molecular biology work, and drafted the manuscript. HI - Participated in the design of the study, carried out the molecular biology work. TKO - Participated in the design of the study, carried out the molecular biology work. KW - Participated in the design of the study, carried out the molecular biology work. YK - Participated in the design of the study, carried out the molecular biology work. SS - Participated in the design of the study, carried out the molecular biology work. MTI - Participated in the design of the study, carried out the molecular biology work. NM - Participated in the design of the study, carried out the molecular biology work. KI - Participated in the design of the study, carried out the molecular biology work. YF - Participated in the design of the study, carried out the molecular biology work. BSE - Coordinated and conceived the study, being involved in the critical revision of the manuscript for important intellectual content. HK - Coordinated and conceived the study, participated in the design of the study, drafted the manuscript, being involved in the critical revision of the manuscript for important intellectual content. All authors have read and approved the final manuscript.

Acknowledgments
The authors thank Drs. Tamae Ohye and Makiko Tsutsumi for helpful discussions, Mrs. Narumi Kamiya for technical assistance. These studies were supported by a grant-in-aid for Scientific Research from the Ministry of Education, Culture, Sports, Science, and Technology of Japan (H.K.), grants for Research on Intractable Diseases from the Ministry of Health, Labour and Welfare of Japan (H.K, Y.F.), grants CA39926 and funds from the Charles E.H. Upham chair in pediatrics (B.S.E.).

Author details
[1]Division of Molecular Genetics, Institute for Comprehensive Medical Science, Fujita Health University, Toyoake, Aichi 470-1192, Japan. [2]Department of Medical Genetics, Shinshu University School of Medicine, Matsumoto, Nagano 390-8621, Japan. [3]Department of Pediatrics, Dokkyo Medical University Koshigaya Hospital, Koshigaya, Saitama 343-8555, Japan. [4]Department of Pediatrics, Kobe University Graduate School of Medicine, Kobe, Hyogo 650-0017, Japan. [5]Division of Human Genetics, The Children's Hospital of Philadelphia, Philadelphia, PA 19104, USA. [6]Department of Pediatrics, The Perelman School of Medicine of the University of Pennsylvania, Philadelphia, PA 19104, USA.

Received: 11 June 2014 Accepted: 25 July 2014
Published: 13 August 2014

References
1. Sheridan MB, Kato T, Haldeman-Englert C, Jalali GR, Milunsky JM, Zou Y, Klaes R, Gimelli G, Gimelli S, Gemmill RM, Drabkin HA, Hacker AM, Brown J, Tomkins D, Shaikh TH, Kurahashi H, Zackai EH, Emanuel BS: **A palindrome-mediated recurrent translocation with 3:1 meiotic nondisjunction: the t(8;22)(q24.13;q11.21).** *Am J Hum Genet* 2010, **87**:209–218.
2. Kurahashi H, Inagaki H, Ohye T, Kogo H, Tsutsumi M, Kato T, Tong M, Emanuel BS: **The constitutional t(11;22): implications for a novel mechanism responsible for gross chromosomal rearrangements.** *Clin Genet* 2010, **78**:299–309.
3. Carter MT, St Pierre SA, Zackai EH, Emanuel BS, Boycott KM: **Phenotypic delineation of Emanuel syndrome (supernumerary derivative 22 syndrome): clinical features of 63 individuals.** *Am J Med Genet A* 2009, **149**:1712–1721.
4. Liehr T, Cirkovic S, Lalic T, Guc-Scekic M, de Almeida C, Weimer J, Iourov I, Melaragno MI, Guilherme RS, Stefanou EG, Aktas D, Kreskowski K, Klein E, Ziegler M, Kosyakova N, Volleth M, Hamid AB: **Complex small supernumerary marker chromosomes - an update.** *Mol Cytogenet* 2013, **6**:46.
5. Kurahashi H, Shaikh TH, Hu P, Roe BA, Emanuel BS, Budarf ML: **Regions of genomic instability on 22q11 and 11q23 as the etiology for the recurrent constitutional t(11;22).** *Hum Mol Genet* 2000, **9**:1665–1670.
6. Edelmann L, Spiteri E, Koren K, Pulijaal V, Bialer MG, Shanske A, Goldberg R, Morrow BE: **AT-rich palindromes mediate the constitutional t(11;22) translocation.** *Am J Hum Genet* 2001, **68**:1–13.
7. Tapia-Páez I, Kost-Alimova M, Hu P, Roe BA, Blennow E, Fedorova L, Imreh S, Dumanski JP: **The position of t(11;22)(q23;q11) constitutional translocation breakpoint is conserved among its carriers.** *Hum Genet* 2001, **109**:167–177.
8. Kurahashi H, Emanuel BS: **Long AT-rich palindromes and the constitutional t (11;22) breakpoint.** *Hum Mol Genet* 2001, **10**:2605–2617.
9. Kurahashi H, Inagaki H, Hosoba E, Kato T, Ohye T, Kogo H, Emanuel BS: **Molecular cloning of a translocation breakpoint hotspot in 22q11.** *Genome Res* 2007, **17**:461–469.
10. Bzymek M, Lovett ST: **Evidence for two mechanisms of palindrome-stimulated deletion in Escherichia coli: single-strand annealing and replication slipped mispairing.** *Genetics* 2001, **158**:527–540.
11. Lobachev KS, Gordenin DA, Resnick MA: **The Mre11 complex is required for repair of hairpin-capped double-strand breaks and prevention of chromosome rearrangements.** *Cell* 2002, **108**:183–193.
12. Cunningham LA, Coté AG, Cam-Ozdemir C, Lewis SM: **Rapid, stabilizing palindrome rearrangements in somatic cells by the center-break mechanism.** *Mol Cell Biol* 2003, **23**:8740–8750.
13. Kurahashi H, Emanuel BS: **Unexpectedly high rate of de novo constitutional t(11;22) translocations in sperm from normal males.** *Nat Genet* 2001, **29**:139–140.
14. Kurahashi H, Inagaki H, Ohye T, Kogo H, Kato T, Emanuel BS: **Palindrome-mediated chromosomal translocations in humans.** *DNA Repair (Amst)* 2006, **5**:1136–1145.
15. Kurahashi H, Inagaki H, Ohye T, Kogo H, Kato T, Emanuel BS: **Chromosomal translocations mediated by palindromic DNA.** *Cell Cycle* 2006, **5**:1297–1303.
16. Gotter AL, Nimmakayalu MA, Jalali GR, Hacker AM, Vorstman J, Conforto Duffy D, Medne L, Emanuel BS: **A palindrome-driven complex rearrangement of 22q11.2 and 8q24.1 elucidated using novel technologies.** *Genome Res* 2007, **17**:470–481.
17. Inagaki H, Ohye T, Kogo H, Yamada K, Kowa H, Shaikh TH, Emanuel BS, Kurahashi H: **Palindromic AT-rich repeat in the NF1 gene is hypervariable in humans and evolutionarily conserved in primates.** *Hum Mutat* 2005, **26**:332–342.
18. Richardson C, Jasin M: **Frequent chromosomal translocations induced by DNA double-strand breaks.** *Nature* 2000, **405**:697–700.
19. Kato T, Franconi CP, Sheridan MB, Hacker AM, Inagakai H, Glover TW, Arlt MF, Drabkin HA, Gemmill RM, Kurahashi H, Emanuel BS: **Analysis of the t(3;8) of hereditary renal cell carcinoma: a palindrome-mediated translocation.** *Cancer Genet* 2014, **207**:133–140.
20. Kato T, Inagaki H, Yamada K, Kogo H, Ohye T, Kowa H, Nagaoka K, Taniguchi M, Emanuel BS, Kurahashi H: **Genetic variation affects de novo translocation frequency.** *Science* 2006, **311**:971.
21. Tong M, Kato T, Yamada K, Inagaki H, Kogo H, Ohye T, Tsutsumi M, Wang J, Emanuel BS, Kurahashi H: **Polymorphisms of the 22q11.2 breakpoint region influence the frequency of de novo constitutional t(11;22)s in sperm.** *Hum Mol Genet* 2010, **19**:2630–2637.
22. Kurahashi H, Shaikh TH, Zackai EH, Celle L, Driscoll DA, Budarf ML, Emanuel BS: **Tightly clustered 11q23 and 22q11 breakpoints permit PCR-based**

detection of the recurrent constitutional t(11;22). *Am J Hum Genet* 2000, **67**:763–768.
23. Kato T, Inagaki H, Kogo H, Ohye T, Yamada K, Emanuel BS, Kurahashi H: **Two different forms of palindrome resolution in the human genome: deletion or translocation.** *Hum Mol Genet* 2008, **17**:1184–1191.
24. Kurahashi H, Inagaki H, Kato T, Hosoba E, Kogo H, Ohye T, Tsutsumi M, Bolor H, Tong M, Emanuel BS: **Impaired DNA replication prompts deletions within palindromic sequences, but does not induce translocations in human cells.** *Hum Mol Genet* 2009, **18**:3397–3406.
25. Voineagu I, Narayanan V, Lobachev KS, Mirkin SM: **Replication stalling at unstable inverted repeats: interplay between DNA hairpins and fork stabilizing proteins.** *Proc Natl Acad Sci U S A* 2008, **105**:9936–9941.
26. Hastings PJ, Lupski JR, Rosenberg SM, Ira G: **Mechanisms of change in gene copy number.** *Nat Rev Genet* 2009, **10**:551–564.
27. Tanaka H, Bergstrom DA, Yao MC, Tapscott SJ: **Widespread and nonrandom distribution of DNA palindromes in cancer cells provides a structural platform for subsequent gene amplification.** *Nat Genet* 2005, **37**:320–327.
28. Ohye T, Inagaki H, Kogo H, Tsutsumi M, Kato T, Tong M, Macville MV, Medne L, Zackai EH, Emanuel BS, Kurahashi H: **Paternal origin of the de novo constitutional t(11;22)(q23;q11).** *Eur J Hum Genet* 2010, **18**:783–787.
29. Thomas NS, Morris JK, Baptista J, Ng BL, Crolla JA, Jacobs PA: **De novo apparently balanced translocations in man are predominantly paternal in origin and associated with a significant increase in paternal age.** *J Med Genet* 2010, **47**:112–115.
30. Hsiao MC, Piotrowski A, Alexander J, Callens T, Fu C, Mikhail FM, Claes KB, Messiaen L: **Palindrome-mediated and replication-dependent pathogenic structural rearrangements within the NF1 Gene.** *Hum Mutat* 2014, **35**:891–898.
31. Kehrer-Sawatzki H, Häussler J, Krone W, Bode H, Jenne DE, Mehnert KU, Tümmers U, Assum G: **The second case of a t(17;22) in a family with neurofibromatosis type 1: sequence analysis of the breakpoint regions.** *Hum Genet* 1997, **99**:237–247.
32. Kurahashi H, Shaikh T, Takata M, Toda T, Emanuel BS: **The constitutional t (17;22): another translocation mediated by palindromic AT-rich repeats.** *Am J Hum Genet* 2003, **72**:733–738.
33. Inagaki H, Ohye T, Kogo H, Tsutsumi M, Kato T, Tong M, Emanuel BS, Kurahashi H: **Two sequential cleavage reactions on cruciform DNA structures cause palindrome-mediated chromosomal translocations.** *Nat Commun* 2013, **4**:1592.

doi:10.1186/s13039-014-0055-x
Cite this article as: Mishra *et al.*: **Breakpoint analysis of the recurrent constitutional t(8;22)(q24.13;q11.21) translocation.** *Molecular Cytogenetics* 2014 **7**:55.

SCIENTIFIC REPORTS

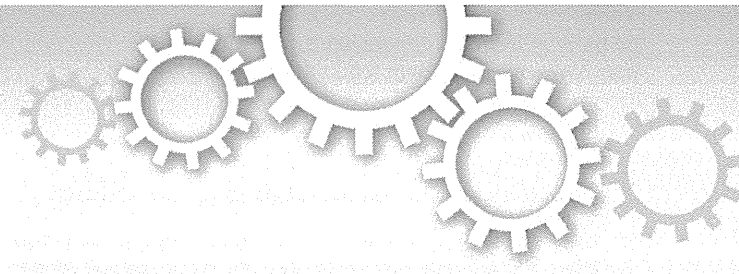

OPEN

SUBJECT AREAS:
CYTOGENETICS
HERPES VIRUS

Received
13 November 2013

Accepted
17 March 2014

Published
2 April 2014

Correspondence and requests for materials should be addressed to H.K. (kura@fujita-hu.ac.jp)

Dual roles for the telomeric repeats in chromosomally integrated human herpesvirus-6

Tamae Ohye[1], Hidehito Inagaki[1], Masaru Ihira[2,3], Yuki Higashimoto[2,4], Koji Kato[5], Junko Oikawa[6], Hiroshi Yagasaki[7], Takahiro Niizuma[8,9], Yoshiyuki Takahashi[10], Seiji Kojima[10], Tetsushi Yoshikawa[2] & Hiroki Kurahashi[1]

[1]Division of Molecular Genetics, Institute for Comprehensive Medical Science, Fujita Health University, Toyoake, Aichi 470-1192, Japan, [2]Department of Pediatrics, Fujita Health University School of Medicine, Toyoake, Aichi 470-1192, Japan, [3]Faculty of Clinical Engineering, Fujita Health University School of Health Sciences, Toyoake, Aichi 470-1192, Japan, [4]Department of Laboratory Medicine, Fujita Health University Hospital, Toyoake, Aichi 470-1192, Japan, [5]Department of Hematology and Oncology, Children's Medical Center, Japanese Red Cross Nagoya First Hospital, Nagoya, Aichi 453-8511, Japan, [6]Department of Pediatrics, Chiba University School of Medicine, Chiba, Chiba 260-8670, Japan, [7]Department of Pediatrics, School of Medicine, Nihon University, Itabashi-ku, Tokyo 173-8610, Japan, [8]Department of Pediatrics, Koshigaya Municipal Hospital, Koshigaya, Saitama 343-8577, Japan, [9]Department of Pediatrics, Tokyo Rinkai Hospital, Edogawa-ku, Tokyo 134-0086, Japan, [10]Department of Pediatrics, Nagoya University Graduate School of Medicine, Nagoya, Aichi 466-8550, Japan.

Approximately 1 percent of healthy individuals carry human herpesvirus-6 within a host chromosome. This is referred to as chromosomally integrated herpesvirus-6 (CIHHV-6). In this study, we investigated the chromosomal integration site in six individuals harboring CIHHV-6B. Using FISH, we found that HHV-6B signals are consistently located at the telomeric region. The proximal endpoints of the integrated virus were mapped at one of two telomere-repeat-like sequences (TRSs) within the DR-R in all cases. In two cases, we isolated junction fragments between the viral TRS and human telomere repeats. The distal endpoints were mapped at the distal TRS in all cases. The size of the distal TRS was found to be ~5 kb which is sufficient to fulfill cellular telomeric functions. We conclude that the viral TRS in the DR regions fulfill dual functions for CIHHV-6: homology-mediated integration into the telomeric region of the chromosome and neo-telomere formation that is then stably transmitted.

Human herpesvirus 6 (HHV-6) is one of the best characterized family members of the nine human herpesviruses. HHV-6 is classified as two distinct species, designated HHV-6A and HHV-6B, with an overall nucleotide sequence identity of 90%[1–3]. It has been demonstrated that primary HHV-6B infection occurs in infancy and causes a common febrile exanthematous illness, exanthem subitum[4,5]. However, neither the clinical features of primary HHV-6A infection nor the diseases directly associated with it have been identified to date. Following primary infection, HHV-6 remains latent in monocytes/macrophages and persists in the salivary glands[6,7]. In transplant recipients, HHV-6B reactivation can cause several clinical conditions such as encephalitis, bone marrow suppression, and pneumonitis[8,9].

Accumulating evidence now indicates that a subset of normal healthy individuals carry the HHV-6 genome within their chromosomes, which is known as chromosomally integrated herpesvirus-6 (CIHHV-6)[10]. The virus genome in these cases is transmitted by Mendelian inheritance. The integrated virus itself does not appear to be pathogenic, but CIHHV-6 carriers are often identified as high-titer virus carriers during screenings for HHV-6 reactivation in immunocompromised hosts. The presence of CIHHV-6 is not a rare condition with a reported incidence in healthy individuals of 1% in Caucasians and 0.21% in Japanese populations[11–13].

Based on consistently detectable FISH signals at chromosome ends in all previously analyzed independent CIHHV-6 cases, it had been speculated that the HHV-6 viral genome is integrated into human telomeres through an unknown mechanism that is specific to HHV-6[14]. The HHV-6 genome comprises a linear double stranded DNA of 159 kb flanked by identical 8 kb direct repeats at the left and right ends (DR-L and DR-R). Each DR contains two human telomere repeat (TTAGGG)-like sequences (TRS) proximal to both ends of the DRs[15,16]. The function of these motifs is uncertain, but it is not unreasonable to hypothesize that they plays a role in protection of viral genome ends from host defense systems such as nucleases in a similar manner to the telomere protection

from DNA end repair systems in eukaryotes[17]. Recently, sequence analysis of the junction fragments of three individuals with CIHHV-6A revealed that the HHV-6 genome was directly joined with the human telomeric region via TTAGGG repeats in each case[18]. A homology-directed mechanism operated by host DNA damage repair response pathways such as homologous recombination is likely to mediate these rearrangements[19].

To further elucidate the mechanism of the viral integration into the human telomeres, we investigated the integration sites in six Japanese individuals harboring CIHHV-6B.

Results

Six cases that were suspected to CIHHV-6B by having genome-equivalent copy number of viral DNA in peripheral blood samples estimated by qPCR were analyzed[20]. Standard cytogenetic evaluations revealed no abnormalities in any of these subjects. FISH analysis with a HHV-6 genomic DNA probe detected virus-specific signals on the long arm of chromosome 22 in two cases (cases 18 and 19), on the long arm of chromosome 6 in one case (case 31), and on the short arm of chromosome X in the two cases (cases 28 and 63) (Fig. 1b–d). The mother of case 19 (case 20) was also analyzed and showed HHV-6 signals on the long arm of chromosome 22. Thus, a CIHHV-6B diagnosis was confirmed in all six study subjects. CIHHV-6B FISH signals were detectable on only one of the homologues in each case, suggesting that all six individuals were heterozygotes in terms of viral integration. HHV-6 signals were consistently detected at the end of the chromosomes, presumably at the telomeric regions, in all six cases.

To next determine the structure of the integrated viral genome in our subjects, we performed MLPA experiments which allowed us to determine copy number of the target sites of the viral genome relative to the chromosomal DNA in each case. The copy numbers for the UL regions were constant and similar to the chromosomal regions used as references (Fig. 2), suggesting that a single copy of the viral genome was integrated within the chromosomal DNA in our CIHHV-6 cases. Copy numbers for the DRs varied among the subjects; two-fold higher than those for the UL regions in cases 18, 19, and 20, three-fold higher in case 28, and at a similar level in case 31.

To map the breakpoints of the HHV-6 integration in more detail in our subjects, Southern analyses using several HHV-6 probes were performed. Since the two TRS regions in the DR-R are good candidates for viral integration breakpoints, DR probes located near to the TRS-2 site were used (Supplementary Fig. S1). These DR probes yielded two distinct bands of a similar intensity (Fig. 3a). One of the bands was detected at a similar position in all cases with a size that was expected for the DR-L, suggesting that the DR-L was intact. The sizes of second band were different in each case, although two cases that were found to carry the HHV-6B at the long arm of chromosome 22 showed a second band of similar size. This suggests that these fragments included the junction between the viral and human genome. According to the restriction map, the breakpoints were predicted to be located within the TRS-2. A similar band pattern in two cases with a 22q integration indicated a common founder for this integration event. The fact that two bands were detectable in these analyses suggests that the entire viral genome was inserted together with both the DR-L and DR-R. The fact that the intensities of the two detected bands were similar further supports the idea that only a single copy of entire HHV-6B genome had been inserted in each individual.

We next attempted to isolate the junction fragments and could fortunately rely on sequence information for the subtelomere-telomere junction in the Xp region. First, we performed PCR using a primer designed to amplify the subtelomeric region flanking the telomere repeats and a primer that recognized the UL region just outside of the DR-R. The amplification reactions appeared to yield no product, but subsequent Southern hybridization analysis detected

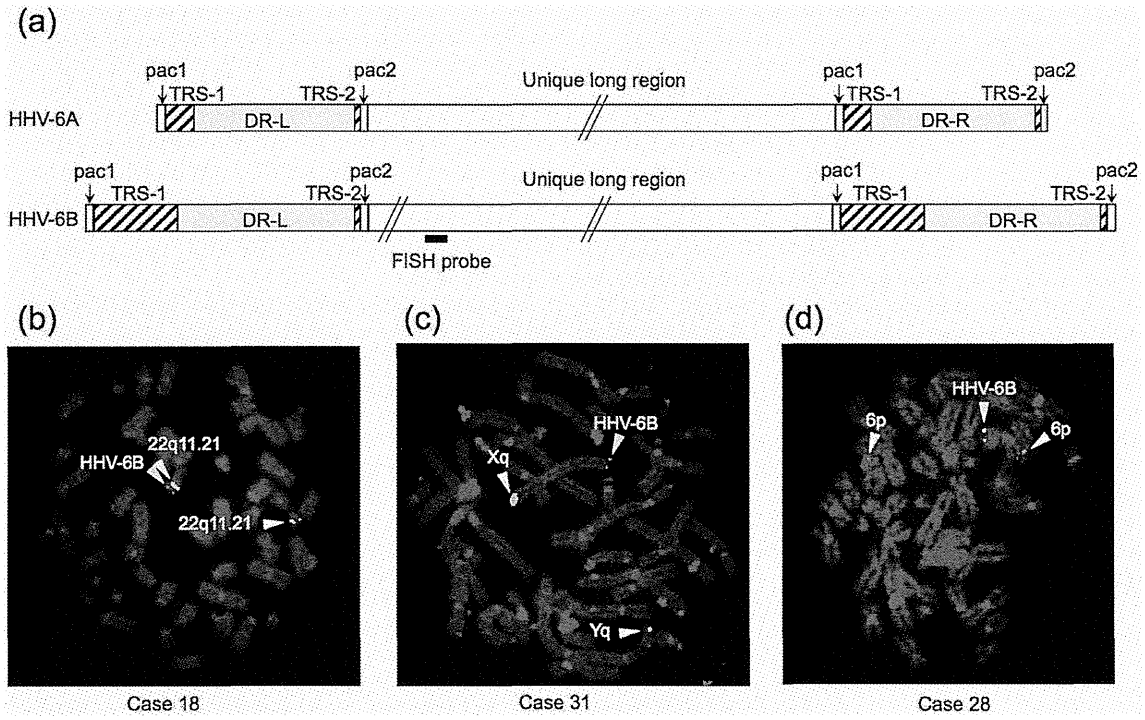

Figure 1 | Characterization of CIHHV-6B by FISH. (a) Schematic representation of the HHV-6 genomic structure. The 10 kb Pst I fragment used as s FISH probe is indicated. Gray boxes indicate DR sites and hatched boxes indicate TRS regions. (b) FISH analyses of metaphase chromosomes derived from the CIHHV-6B study subjects. A signal from the HHV-6B probe is detectable at the end of chromosome 22q (case 18), chromosome 6q (case 31) or chromosome Xp (case 28) (yellow arrowheads). The reference signals for chromosome 22q11.21, 6p and Xq are indicated by white arrowheads.

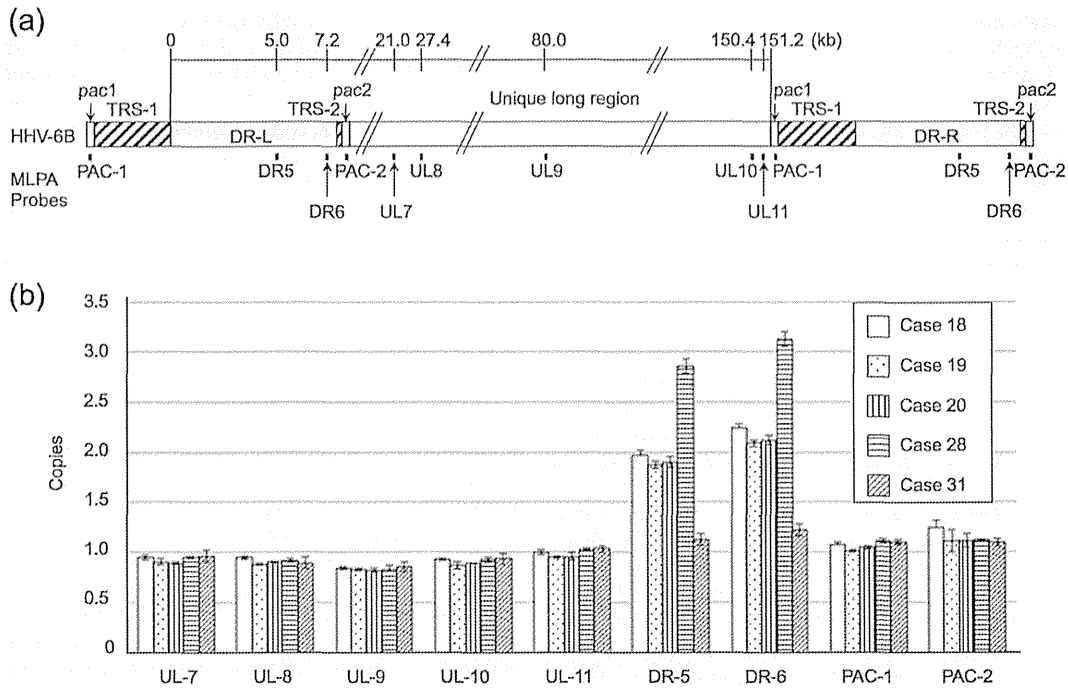

Figure 2 | Analyses of the CIHHV-6B genome structure by MLPA. (a) Schematic representation of the HHV-6B genome. The positions of the MLPA probes are indicated below the diagram. The scale bar indicates the distance from the starting point of DR-L. (b) Results of MLPA analyses. The vertical axis indicates the viral genome copy numbers relative to the single copy human genomic region. Data for cases 18, 19, 20, 28 and 31 are indicated from left to right.

a fragment exceeding 10 kb in length in case 28 with a HHV-6 integration at chromosome Xp (Fig. 3b). This indicated that the breakpoints of the virus were located within the DR-R. Unfortunately, less sequence information was available for the subtelomeric regions of chromosomes 6q and 22q. We attempted to perform junction PCR using a primer that bound to the most distal end of the reported subtelomeric sequence and a primer that recognized a region just outside of the DR-R, but no amplicon was obtained. We also tried inverse PCR but failed, because a short PCR product derived from short TTAGGG repeat present in the DR-L inhibited the amplification of real junction.

To further narrow down the positions of the HHV-6 breakpoints, multiple PCR primers were designed within the DR. Combined with a subtelomeric primer designed on the basis of sequence information for the Xp subtelomere-telomere junction (hg19, chrX: 60,427–60,445), all of the primers that recognized sites within the DR yielded PCR products of the expected size, which confirmed that the viral breakpoint is located within the TRS-2 (Fig. 3c). Sequencing of these amplicons revealed that the subtelomeric and viral DR-R regions were connected via 166 copies of the TTAGGG repeat, which is much shorter than the typical telomere repeat region in humans (9-15 kb; Fig. 3d) (GenBank accession number AB822541). These PCR experiments also yielded junction products in case 63 who had a HHV-6 integration at chromosome Xp. The sequence of this amplified fragment indicated that the integration sites are identical and the differences in the PCR product sizes was due to varying numbers of telomere repeats.

In one of our study subjects (case 31), the results of MLPA revealed only one copy of the DR, which was a similar level to the UL. Southern hybridization results for case 31 also produced a distinct pattern. A DR probe detected no bands corresponding to the DR-R, but constant bands only corresponding to the DR-L, suggesting that the TRS-2 had been deleted and that the HHV-6 breakpoint is located at a more distal region in this subject (Fig. 3a). Since TRS-1 is another candidate for the viral breakpoint, PCR for this region was performed using a DR primer flanking the TRS-1 site and a primer that was located just outside of the DR-R. No PCR product was obtained for case 31 although a TRS-1 amplicon was obtained in all other subjects, suggesting that the breakpoint in this one subject was located within the TRS-1 site in the DR-R (Supplementary Fig. S2a). Unexpectedly, the sizes of the TRS-1 PCR products from other cases were much larger (~5 kb) than that reported in the database (~300 bp), and also than TRS-2 (~500 bp). Although TRS-1 is referred to as heterogeneous $(TTAGGG)_n$ due to the reported presence of imperfect repeats, sequence analyses of our study subjects revealed a much longer stretch of perfect TTAGGG repeats than has been previously reported for the TRS-1 site, and greater also than those of TRS-2.

In case 28, MLPA results revealed a three-fold higher copy number for the DR compared with the UL region. Southern analyses further demonstrated the presence of additional DR copies in this subject, evidenced by three distinct bands (Fig. 3a). Sizes of the restriction fragments detected by DR probes suggested a proximal-DR-DR-UL-DR-distal structure within the genome of this individual (Supplementary Fig. S1, S3, and S4). To reveal the junction of the two distal DRs in this case, we performed PCR encompassing the TRS-2 – pac2 – pac1 – TRS-1 region. Only case 28 yielded a junction-specific PCR product that was also yielded from the subject including the replicating HHV-6B obtained from patients with exanthema subitum (Supplementary Fig. S5a). However, sequence analyses revealed that the junction between the two DRs in case 28 did not include pac1 or pac2, although the junction from the replicating HHV-6B carried the pac1 and pac2 regions.

To determine the structure of the other end of the HHV-6B genome, we mapped the endpoint of the viral genome within the DR-L. PCR amplification of the TRS-2 site in the DR-L was performed, and amplicons were obtained for all of our CIHHV-6B subjects. This suggested that the TRS-2 region in the DR-L had remained intact